

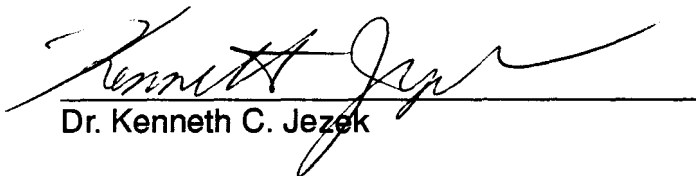
Detection of Melt Events on the West Antarctic Ice Sheet

By

**Derrick J. Lampkin
1995**

**Submitted as partial fulfillment of
the requirements for the degree of
Bachelor of Science in Geology
at The Ohio State University,
Spring Quarter, 1995**

Approved By:



Dr. Kenneth C. Jezek

Table of Contents

	<u>Page</u>
Executive Summary	vi
1.0 Introduction	1
2.0 Passive Microwave Theory	4
3.0 Data Section	6
3.1 SSM/I Data.....	7
3.2 Automatic Weather Station Data.....	8
3.3 Stratigraphic Data.....	9
4.0 Approach	10
5.0 Cross-Polarization Gradient Technique	13
5.1 Application of XPGR to Antarctica.....	14
6.0 Results Section	16
7.0 Ours Vs. Theirs	18
8.0 Comparison of <i>In Situ</i> Data	23
8.1 Calculation of Accumulation Rate.....	24
9.0 Conclusion	26
References	28
Appendices	30
Extract.C program used to extract brightness temperature data from cdrom for specified latitude/longitude and time interval.	
Locate.for program used to convert latitude and longitude coordinates to I, and J polar grid coordinates.	

List of Figures

- Figure 1: Passive microwave image illustrating storm's transit across Marie Byrd Land, West Antarctica from December 14 to December 19, 1988.
- Figure 2: Passive microwave image illustrating location of sites.
- Figure 3: map illustrating location of AWS sites.
- Figure 4: stratigraphic sketch of snow column at Out-B.
- Figure 5: graph of brightness temperature vs. time for 19, 37, and 22 GHz. channels, vertical and horizontal polarizations at Site B.
- Figure 6: graph of T_b vs. Time for 19, 37, and 22 GHz. channels, vertical and horizontal polarizations at Site C.
- Figure 7: graph of T_b and Physical temperature vs. Time of 19 GHz. vertical channel, Site C with data from Gill AWS site.
- Figure 8: graph of T_b and Physical temperature vs. Time of 19 GHz. vertical channel, Site B with data from Martha AWS site.
- Figure 9: graph of T_b vs. Time of 19 vertical and 22 vertical channels at Site B for the month of December 1988.
- Figure 10: graph of T_b vs. Time of 19 vertical and 22 vertical channels at Site C for the month of December 1988.
- Figure 11: composite graph of XPGR vs. Time at Site C from 1988-1991 showing melt threshold and base summer XPGR value.
- Figure 12: composite graph of XPGR vs. Time at Site Out-B from 1988-1991 showing melt threshold and base summer XPGR value.
- Figure 13: graph of XPGR vs. Time at Site C 1988.
- Figure 14: graph of XPGR vs. Time at Site C 1989.
- Figure 15: graph of XPGR vs. Time at Site C 1990.

- Figure 16: graph of XPGR vs. Time at Site C 1991.
- Figure 17: graph of XPGR vs. Time at Site B 1988.
- Figure 18: graph of XPGR vs. Time at Site B 1989.
- Figure 19: graph of XPGR vs. Time at Site B 1990.
- Figure 20: graph of XPGR vs. Time at Site B 1991.
- Figure 21: graph of XPGR vs. Time at Site Out-B 1988.
- Figure 22: graph of XPGR vs. Time at Site Out-B 1989.
- Figure 23: graph of XPGR vs. Time at Site Out-B 1990.
- Figure 24: graph of XPGR vs. Time at Site Out-B 1991.
- Figure 25: graph of XPGR vs. Time at Site D 1988.
- Figure 26: graph of XPGR vs. Time at Site D 1989.
- Figure 27: graph of XPGR vs. Time at Site D 1990.
- Figure 28: graph of XPGR vs. Time at Site D 1991.
- Figure 29: graph of XPGR vs. Time at Site E 1988.
- Figure 30: graph of XPGR vs. Time at Site E 1989.
- Figure 31: graph of XPGR vs. Time at Site E 1990.
- Figure 32: graph of XPGR vs. Time at Site E 1991.
- Figure 33: graph of XPGR vs. Time at Site F 1988.
- Figure 34: graph of XPGR vs. Time at Site F 1989.
- Figure 35: graph of XPGR vs. Time at Site F 1990.
- Figure 36: graph of XPGR vs. Time at Site F 1991.
- Figure 37: composite graph of calculated melt thresholds for all Sites.

Figure 38: graph of XPGR vs. Elevation.

Figure 39: passive microwave image highlighting melt regions (in red) as determined by the Lampkin Melt Technique using an averaged melt threshold value.

List of Tables

	<u>page</u>
<u>Table I:</u> Latitude and Longitude data of Site B, C, D, E, F, and Out-B.	7
<u>Table II:</u> Latitude and Longitude data of AWS Sites.	8
<u>Table III:</u> XPGR melt threshold data and elevation for all sites.	15
<u>Table IV:</u> Melt determining schemes used by various researchers	16

Executive Summary

The identification and tracking of an observed high brightness temperature anomaly in December of 1988, characterized by Tb values approximately 260 to 265 K in transit across Marie Byrd Land West Antarctica, raised the question of whether or not this event was imparting enough energy to the surface to produce melting. This was answered through an analysis of the passive microwave data during the time interval this signature was observed. The use of automatic weather station data and stratigraphic data were utilized to identify and characterize the observed melt event. In order to determine a passive microwave signature that would be indicative of surface melt, other geophysicist's methods were considered (Mote. et al., (1993), and Zwally and Fiegler, (1994)). It was found that a modified Cross-Polarized Gradient Ratio algorithm used by Abdalati Steffen, (1995) was the most appropriate approach. A modified XPGR analysis of the passive microwave data was applied to several sites from 1988 to 1991, in the Marie Byrd Land region. This analysis yielded melt thresholds unique to each site that identified significant melt events in the summer of 1988 and 1991. An averaged XPGR melt threshold from all the sites was calculated (-0.050) and used to construct a map outlining regions that have experienced significant surface melting.

1.0 Introduction

The polar regions are recognized as an important component of Earth's geophysical and biological cycles. On a large scale, the polar regions serve as an enormous heat sink for energy transported northward from the tropics. On a more regional scale the great polar ice sheets serve as vast storehouses of the world's fresh water supply. Release of this supply through the melting of these continental ice sheets could raise the level of the world's oceans approximately 17-35 centimeters with a rise in temperature of 1.5°C by the year 2050 (New Zealand Climate Committee, 1990).

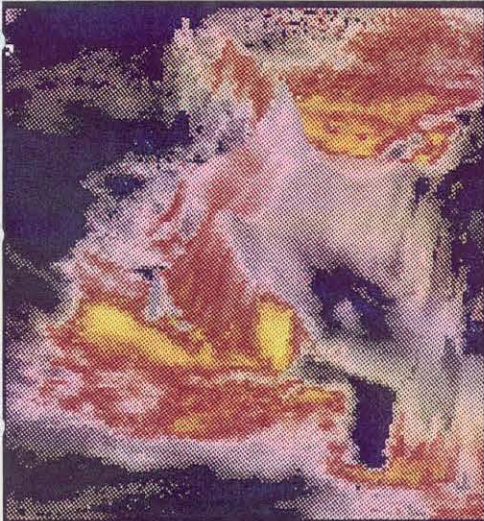
Continental ice sheets respond to changes in the earth system in four ways: 1) changing rate of basal melting at the ice sheet bedrock interface; 2) changing thickening rate due to precipitation variations; 3) variations in surface melting and coastal calving rates; 4) variations in the horizontal and vertical components of ice sheet motion. Remote sensing technology provides exceptional tools for measuring these responses. Remote sensing data sets, such as laser and radar altimeters, provide information about ice topography (Zwally et al, 1983b). Synthetic Aperture Radar (SAR) can be used as an interferometer which can measure ice sheet surface elevation and surface displacement of ice

sheets. SAR is also a useful method for identifying melt zones on the Greenland Ice Sheet and other melt features such as lakes and streams (Bindshadler et al., 1987). Passive microwave data are particularly useful for measuring time series of the extent and patterns of melt. Passive microwave data have been used to monitor and analyze spring melt on the snow-covered open prairie region of western Canada (Walker & Goodison, 1993), and over large sectors of the Greenland Ice Sheet (Shuman et. al.,1994; Abdalati & Steffen,1995). More recently, passive microwave data have been used to map surface melt in Antarctica by Zwally and Fiegler, (1995).

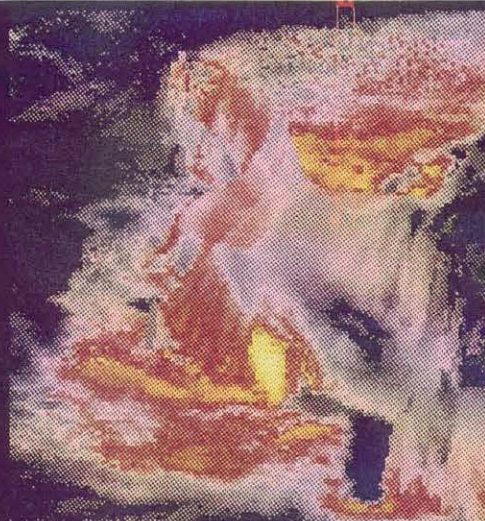
This paper is concerned with interpreting anomalous patterns in passive microwave brightness temperature (T_b) data collected over the West Antarctic ice sheet. The first objective of this research is to verify whether the anomalous T_b patterns are related to surface melting. Next, several techniques for extracting melt events from T_b data are evaluated to determine which is most appropriate for Antarctica. The next objective is to apply the selected method to a test area where melt patterns can be characterized and mapped and where there is ancillary data for validating the analysis. Finally we test a hypothesis that intermittent melt events identified in the passive microwave data can be used to precisely date structural horizons observed in cores and shallow pits.

This information then can be used to calculate the accumulation rates of specified regions over relatively short intervals of time.

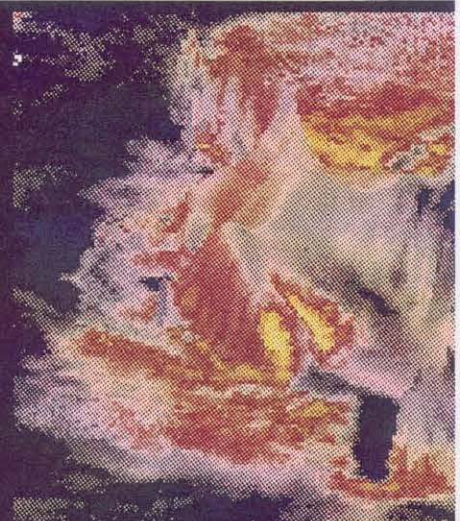
In review, this paper will evaluate various techniques for mapping surface melt events. In particular we modify a method, called the Cross-Polarization Gradient Ratio (XPGR) method which was applied to passive microwave time-series data in Greenland by Abdalati and Steffen, 1995. Our algorithm is a geographically adjusted model, allowing us to apply it in the analysis of events occurring across the continental ice sheet in West Antarctica. We focus on mapping an unusual melt event that occurred during December of 1988 (see figure 1). This passive microwave anomaly was correlated with the stratigraphic record in order to calculate a regional accumulation rate.



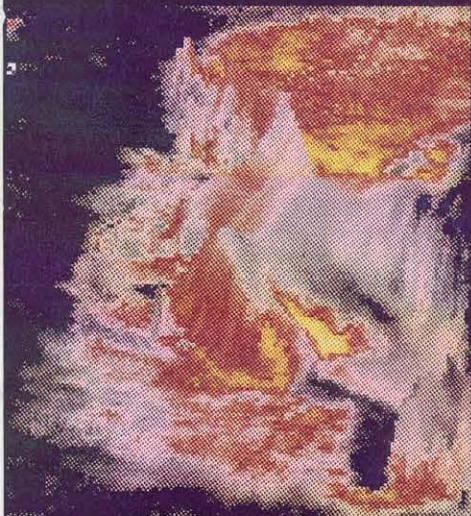
14 December 1988



15 December 1988



16 December 1988



17 December 1988

Passive microwave image illustrating the storm's transit across Marie Byrd Land, West Antarctica from December 14 to December 19, 1988.



19 December 1988

Figure 1.

2.0 Passive Microwave Theory

Passive microwave data are recorded as brightness temperatures, expressed in degrees Kelvin. Electromagnetic energy received by the sensor is described mathematically as a brightness temperature calculated from the depth integral of the product of the physical temperature and the emissivity. This expression is given explicitly as (Zwally, 1977):

$$T_b = \int \partial a \exp [-(\partial s_0 + \partial a)z - sz/2] T(z) dz, \quad (1)$$

where:

T_b = brightness temperature

∂a = absorption coefficient

∂s_0 = scattering coefficient at the surface

s = linear increase of scattering with depth

z = depth below the surface, measured vertically

At a discrete boundary, the expression becomes:

$$T_b = (1 - R)^2 T_{ab} \quad (2)$$

where:

T_b = brightness temperature

R = reflection coefficient

T_{ab} = apparent brightness temperature of the subsurface

and (R) is calculated by the Fresnel equation for lossless material where;

(Rh)-reflection coefficient vertical polarization=

$$\{([n^2 \sin^2 \theta] - \cos^2 \theta) / ([n^2 \sin^2 \theta] + \cos^2 \theta)\}^{1/2}$$

(Rv)-reflection coefficient horizontal polarization=

$$\{([n^2 \cos^2 \theta] - [n^2 \sin^2 \theta]) / ([n^2 \cos^2 \theta] + [n^2 \sin^2 \theta])\}^{1/2}$$

where:

n=index of refraction

θ =angle of incidence (Schanda,1986)

Under the assumption of constant temperature and emissivity, these expression are further simplified to:

$$T_b = T_e \tag{3}$$

where:

T_b=brightness temperature

T=physical temperature

ϵ =emissivity

Emissivity is largely dependant on physical temperature and on the physical properties of snow. For example, snow or firn that undergoes periods of melting and refreezing produce larger grains that lower the emissivity by scattering. Grain size appears to be an important variable driving the emissivity. In dry firn, grain growth and subsequently grain size is dependant on the physical temperature and the compaction rate as determined by the accumulation rate (Gow, 1968). Increases in brightness

temperatures driven by changing grain size are caused by an increase in the accumulation rate or a decrease in the mean annual temperature (Zwally & Gloersen, 1977). When snow or firn is slightly wet, absorption increases and so does brightness temperature. Indeed, for snow wetness less than a few percent, snow begins to act as a black-body and the emissivity approaches 1, consequently brightness temperatures approach (but are generally less than) 273°K . These complex conditions all contribute in some degree to the observed signatures present in the passive microwave data.

3.0 Data Section

The data sets that were acquired and analyzed in this study were;

- Special Sensor Microwave Imager (SSM/I) brightness temperature.
- Temperature and Pressure data from Automatic Weather Stations (AWS).
- In situ observations of firn stratigraphy.

3.1 SSM/I Data.

Passive microwave data were obtained by the Special Sensor Microwave Imager . The SSM/I platform was launched June 19, 1987 continuing data acquisition from the Scanning Multichannel Microwave Radiometer (SMMR) which ended its mission on August 20, 1987. The SSM/I platform occupies a sun-synchronous, near polar orbit with an altitude of 883 km. It has a swath width of 1400 km and a viewing angle of 53.1 degrees (Hollinger et. al.,1987). SSM/I data are recorded at 19GHz, 37GHz, and 22GHz, and 85GHz for vertical and horizontal polarizations. The SSM/I data used in this study cover the time interval between 1988 and 1991. The archived SSM/I data were obtained from the National Snow and Ice Data Center (NSIDC). The data are recorded as brightness temperatures. Pixel dimensions are 25km X 25km and are gridded onto a polar stereographic projection. The brightness temperature value assigned to each grid cell is a product of averaged observations for each day. In this analysis selected coordinates were used to extract brightness temperature data over the specified time interval. Five sites were selected for detailed, time series analysis. They are listed in Table I and plotted in Figure 2.

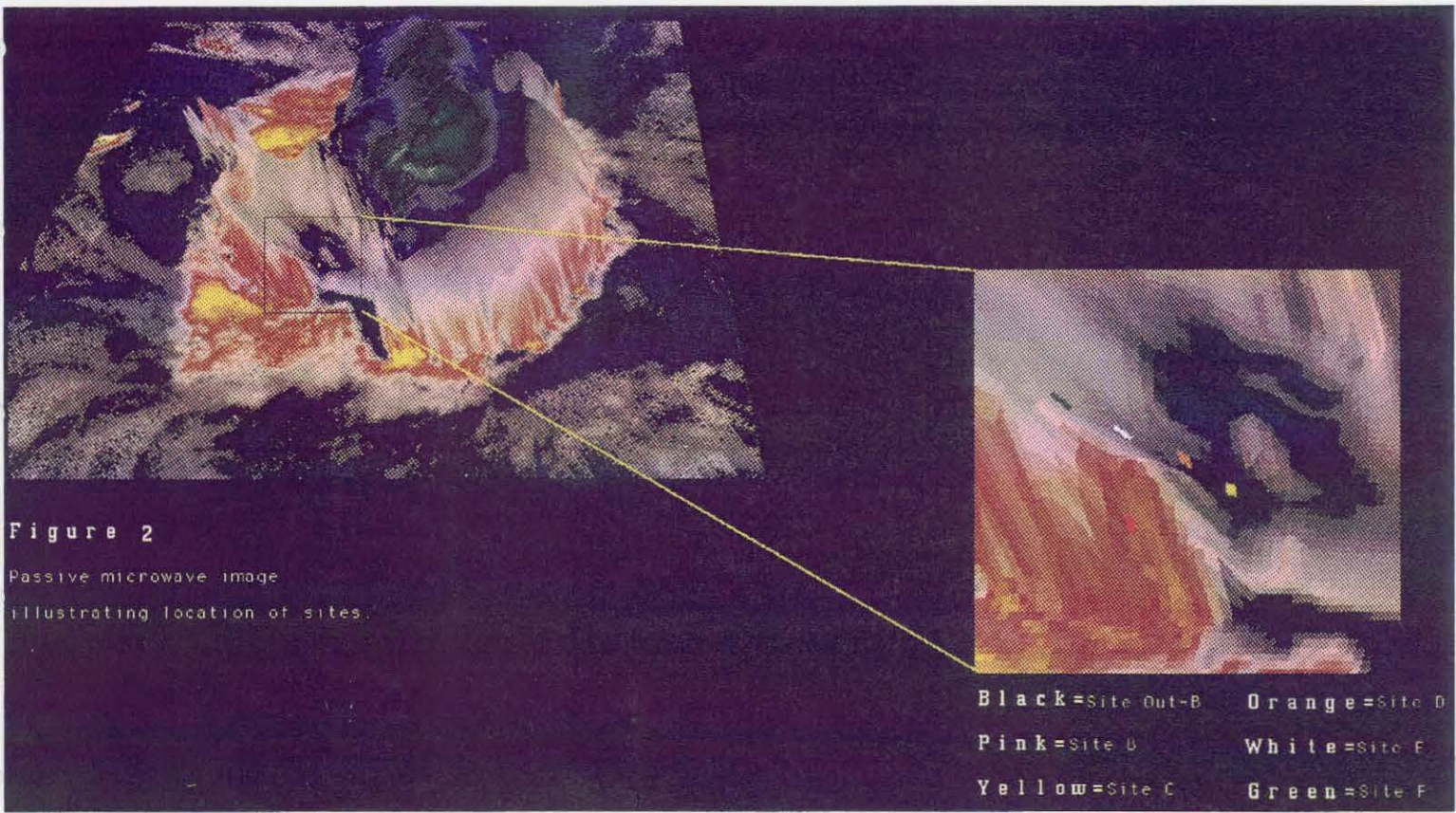


Figure 2

Passive microwave image illustrating location of sites.

Table I:

Site Locations (Passive Microwave Data)

Site	Geographic Location	Latitude/Longitude
B	Ford Ranges	77.5 / 147
C	Ross Ice Shelf	80.3 / 148
D	Rockefeller Plateau	80.0 / 140
E	Marie Byrd Land	79.0 / 140
F	Marie Byrd Land	78.0 / 140
Out-B	Ice Stream B	83.5 / 140

3.2 AWS Data

Automatic Weather Station (AWS) facilities are a network of climatic apparatus that are strategically installed throughout the continent. There are 29 units in all that measure air temperature, wind velocity, humidity, and wind direction at regular intervals. The AWS data in this report were gathered from The Antarctic AWS Data catalog for 1988, an annual publication of the University of Wisconsin, that inventories data for the aforementioned parameters. Table 2 lists the locations of the AWS sites where air temperature and pressure data were obtained (Keller et. al, 1989) see figure 3. These sites are close to anomalous patterns observed in the passive microwave data.

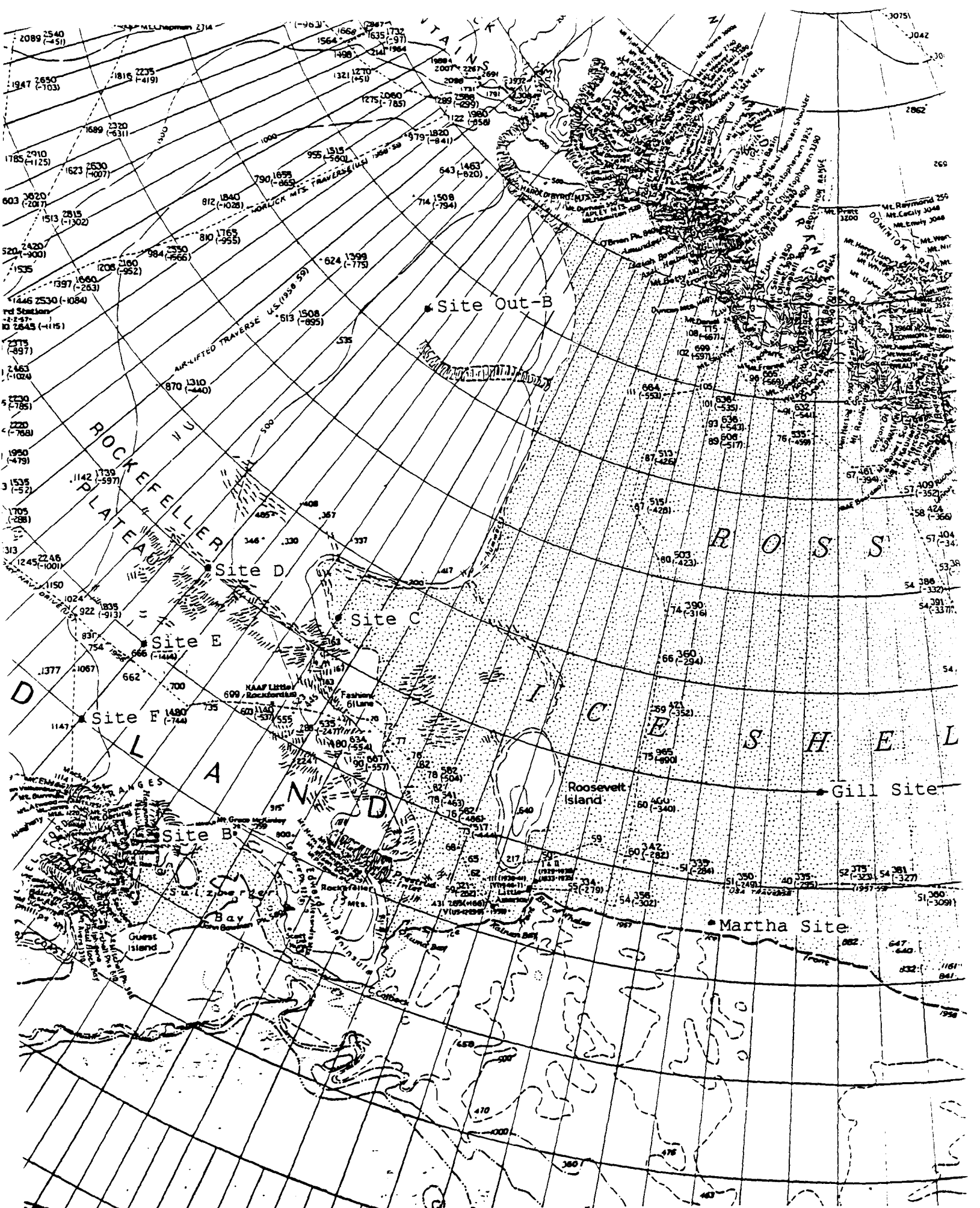


Figure 3. Map illustrating location of AWS sites and passive microwave sites.

Table II: Site Locations (AWS Data)

Site	Geographic Location	Latitude/Longitude
B1	Gill Station:Ross Ice Shelf	80.0 / 179
C1	Martha Station:Ross Ice Shelf	78.4 / 173.4

3.3 Stratigraphic Data

These data were obtained from several shallow pits located at Out-B which is shown on the map in figure (3). It is a remote field camp on the flanks of Ice Stream-B, Marie Byrd Land. The data were collected during the 1993-94 Antarctic field season. Two pits were excavated at various location in close proximity to the Out-B camp. Out of the two pits, three walls were shaved, and sketched. Temperature data of the snow column from each wall were obtained in 10cm increments. The pit used in this analysis was 1.3 meters deep. We noted four types of firn structures.

These structures were:

- Amorphous dense ice crusts (Thickness < 1mm)
- Amorphous dense ice crusts (Thickness > 1mm)
- Small grain size/dense strata: characterized by small crystal~ less than 1m with small pore spaces.

- Large grain size/large pore spaces: characterized by large crystals~ 3 to 4 mm with large pore spaces.

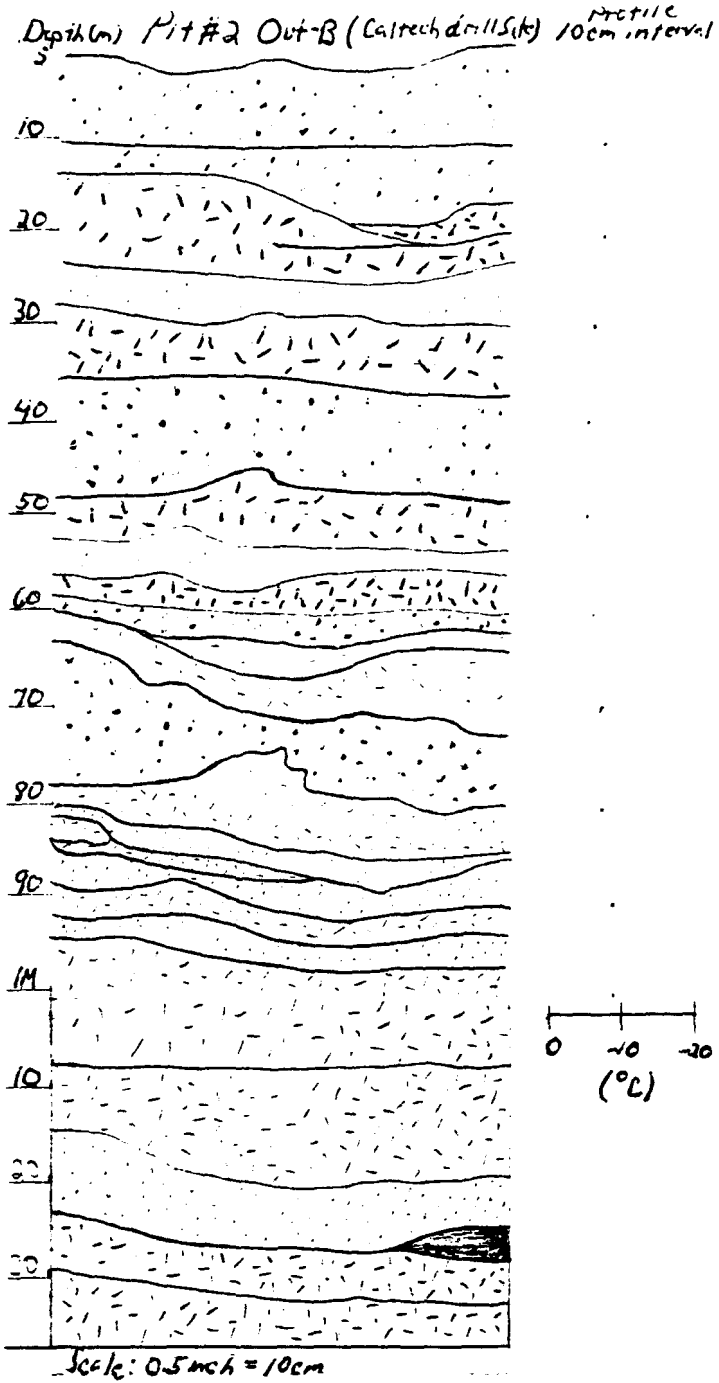
The stratigraphic information was used to identify melt events observed in the passive microwave data in the snow stratigraphy (see figure 4).

4.0 Approach

We posed three questions for developing an approach for interpreting brightness temperature patterns in our study area, these were:

- Are high brightness temperature values in the passive microwave data evidence of melting?
- Is the observed passive microwave signature due totally or partially to atmospheric effects?
- Is the observed phenomena reoccurring spatially and temporally?

Based on those questions, we adopted the following approach: 1) select a study area; 2) analyze the passive microwave data to determine a method to detect surface melting; 3) monitor the passive microwave data over time in order to compare with other time series data sets, such



- Legend**
- Thickness ~ (< 1mm)
Amorphous Dense ice Crust
 - Thickness ~ (> 1mm)
Amorphous Dense ice Crust
 - Small Grain Size / Dense layers
 - Large Grain Size / Large Pore Space layers

Time: —
 Date: 12/4/93
 Location: Out-B (Caltech Site)
 Weather: Overcast
 Air Temperature ~ -10 °C

Figure 4. Stratigraphic sketch of snow column at Out-B Research field camp.

as AWS data. From this we seek to validate our melt detection method and monitor the frequency and extent of melt events occurring in West Antarctica.

We chose the Amundsen/Bellingshausen sea sector of the West Antarctic Ice Sheet as our study area. Our choice was based on the existence of large amounts of data in this region collected in situ by other Ohio State University investigators. It was also based on an observation by Wilson and Jezek (1993) of a pattern of anomalous brightness temperatures that swept across this area in 1988. As shown in Figure 1, a region of warm (yellow) brightness temperature appears seaward of the coastline on December 13. The patterns press southward, eventually penetrating into Marie Byrd Land on December 16. Brightness temperatures in the interior part of the event approach 270 °K.

Time-series graphs of T_b were constructed to characterize the brightness temperature anomaly event in the various channels. Figures 5 and 6 are passive microwave time-series graphs of brightness temperature vs. time. The time interval spans the month of December, 1988. These graphs show the transit of the storm phenomena across Sites B and C located in Marie Byrd Land, West Antarctica. These figures demonstrate the relatively constant behavior of the various channels at the beginning of the month. By day 13 or 14, a rapid increase in brightness

Time Series Data:Site B 1988

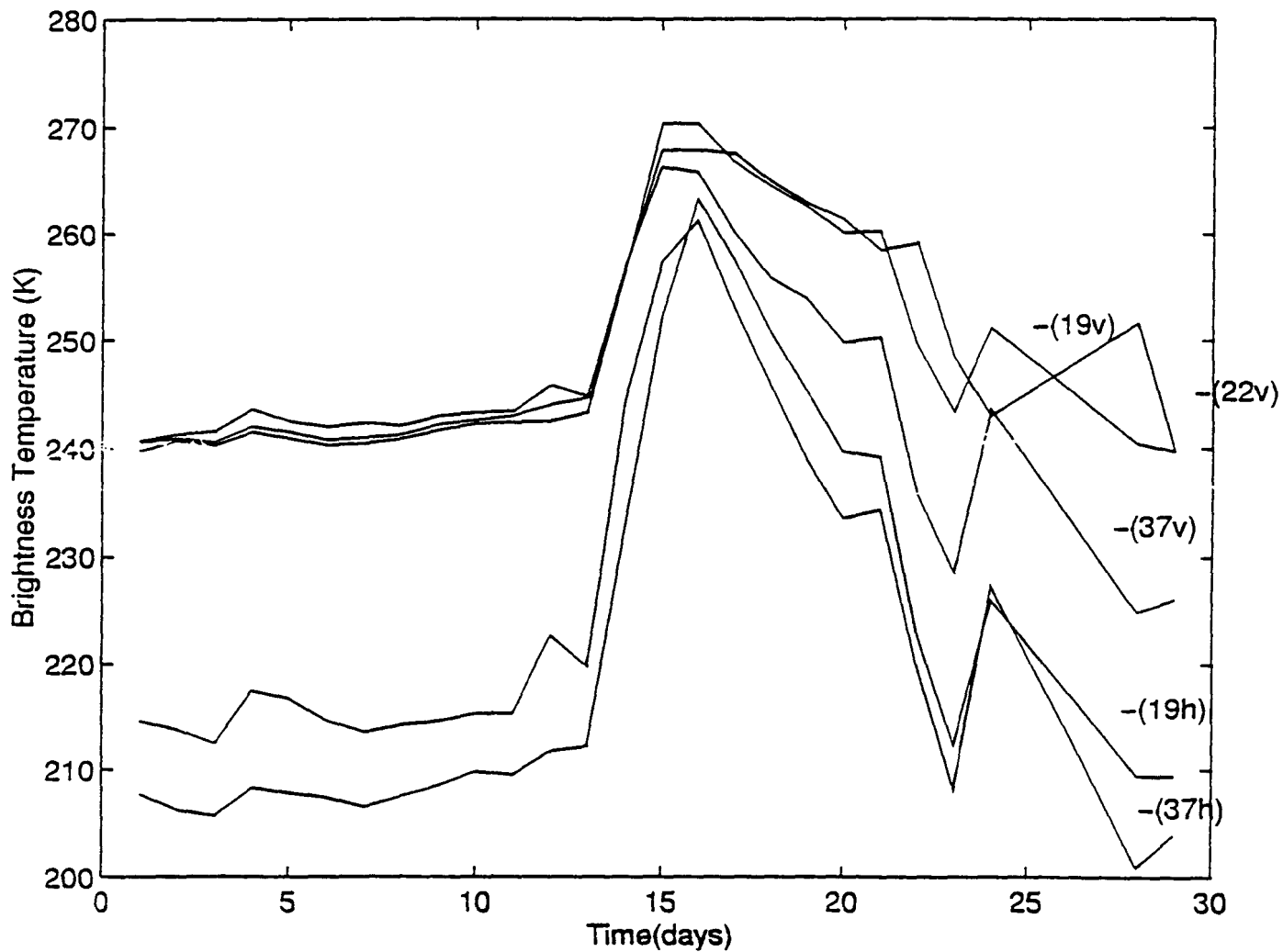


Figure 5. Graph of brightness temperature vs. time for 19, 37, and 22 GHz, vertical and horizontal polarizations at Site B.

Site C-All Frequencies

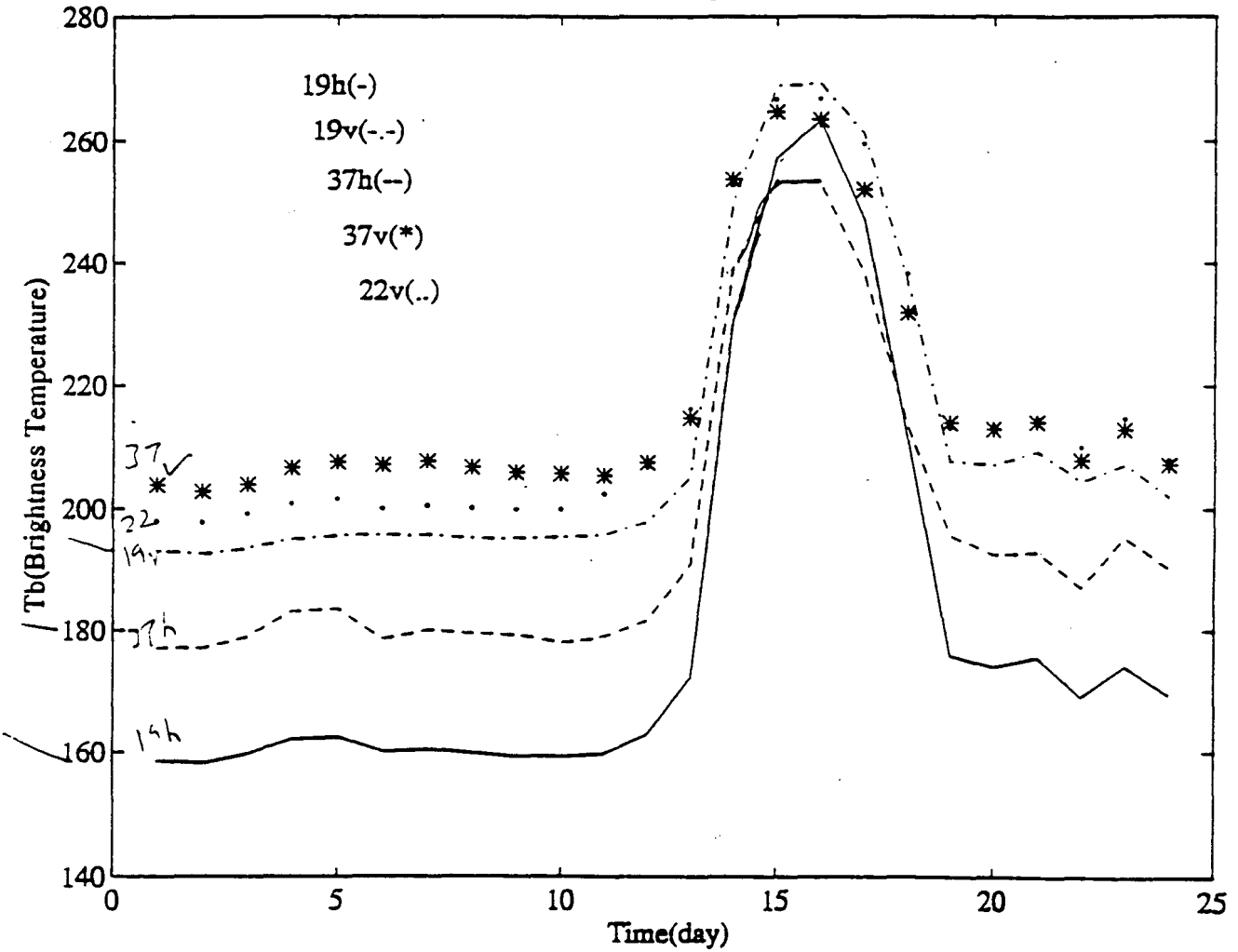


Figure 6. Graph of brightness temperature vs. time for 19, 37, and 22 GHz, vertical and horizontal polarizations at Site C.

temperatures occurs on the order of 60K for all channels. The high Tb event evident in the passive microwave data also occurs in the AWS data (figure 7 & 8). In figure 7 a marked increase in physical temperature on the order of 10 C occurs during the same time interval as the increase in the Tb data. The same behavior is evident in figure 8. Prior to melt, the highest frequency vertical channels show the warmest temperatures (figures 5 and 6). This behavior is due to the fact that penetration depth decreases with increasing frequency, hence the lower frequency channels are sensing part of the cold winter snow. During melt, the ordering reverses. Here we speculate that the increasing influence of surface roughness on the higher frequency channels drives a corresponding decrease in brightness temperature. Evidence present in both the AWS data and the passive microwave data supports the notion that this high Tb anomaly is a consequence of a warm air mass system. Presence of warm air raises the question of whether or not the increase observed in the passive microwave data is attributable to surface melting or the presence of atmospheric water vapor or precipitation. Figures 9 and 10 are plots of 19GHz vertical and 22GHz. vertical channels vs. time at Sites B and C. The 22v channel is more sensitive to the presence of atmospheric water vapor than the 19v channel. Both channels will sense increased radiation from a wet snow surface (Manual of Remote Sensing vol. I, 1983). The

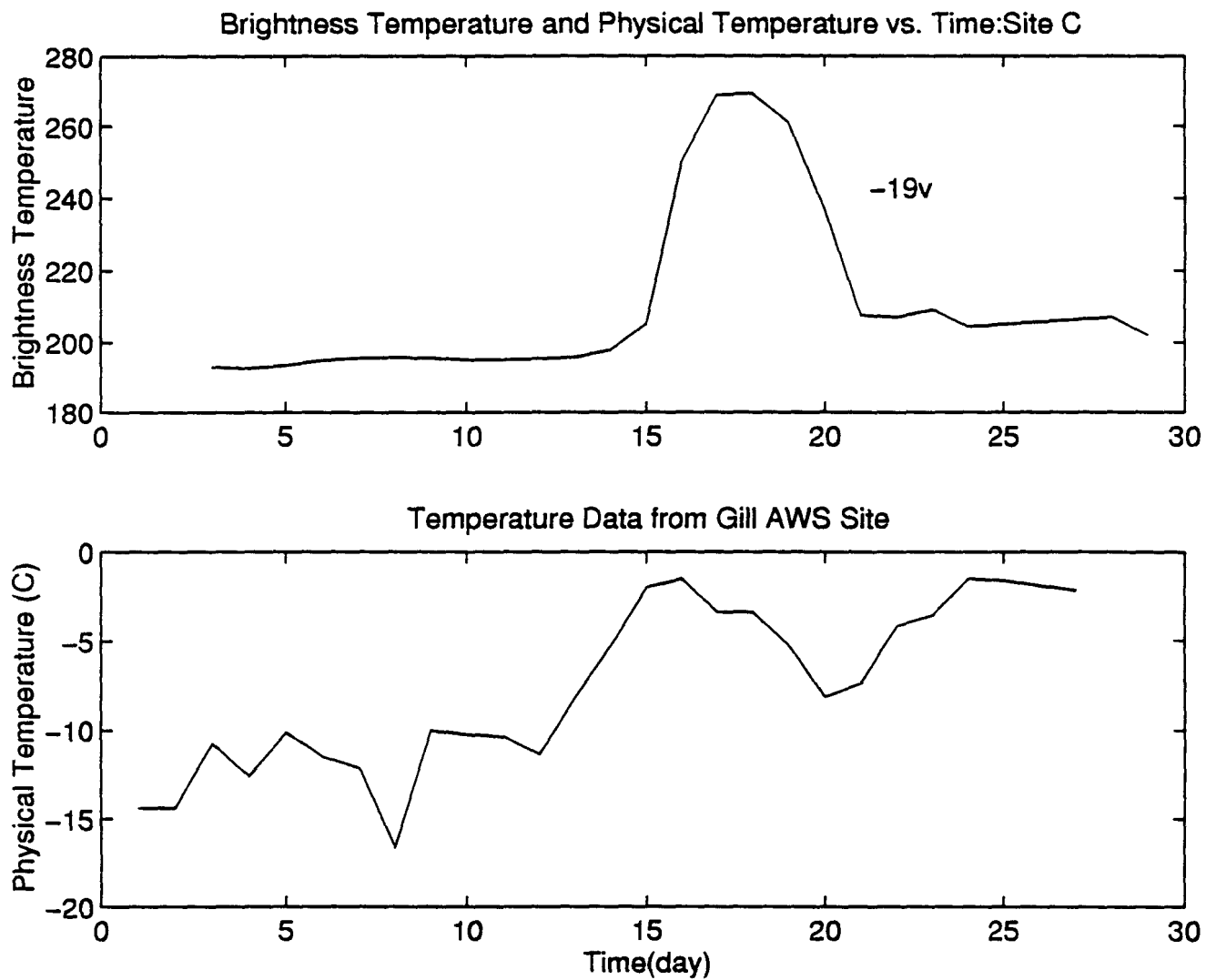


Figure 7. Graph of brightness temperature and physical temperature vs. time of 19GHz. vertical channel, Site C with data from Gill AWS site.

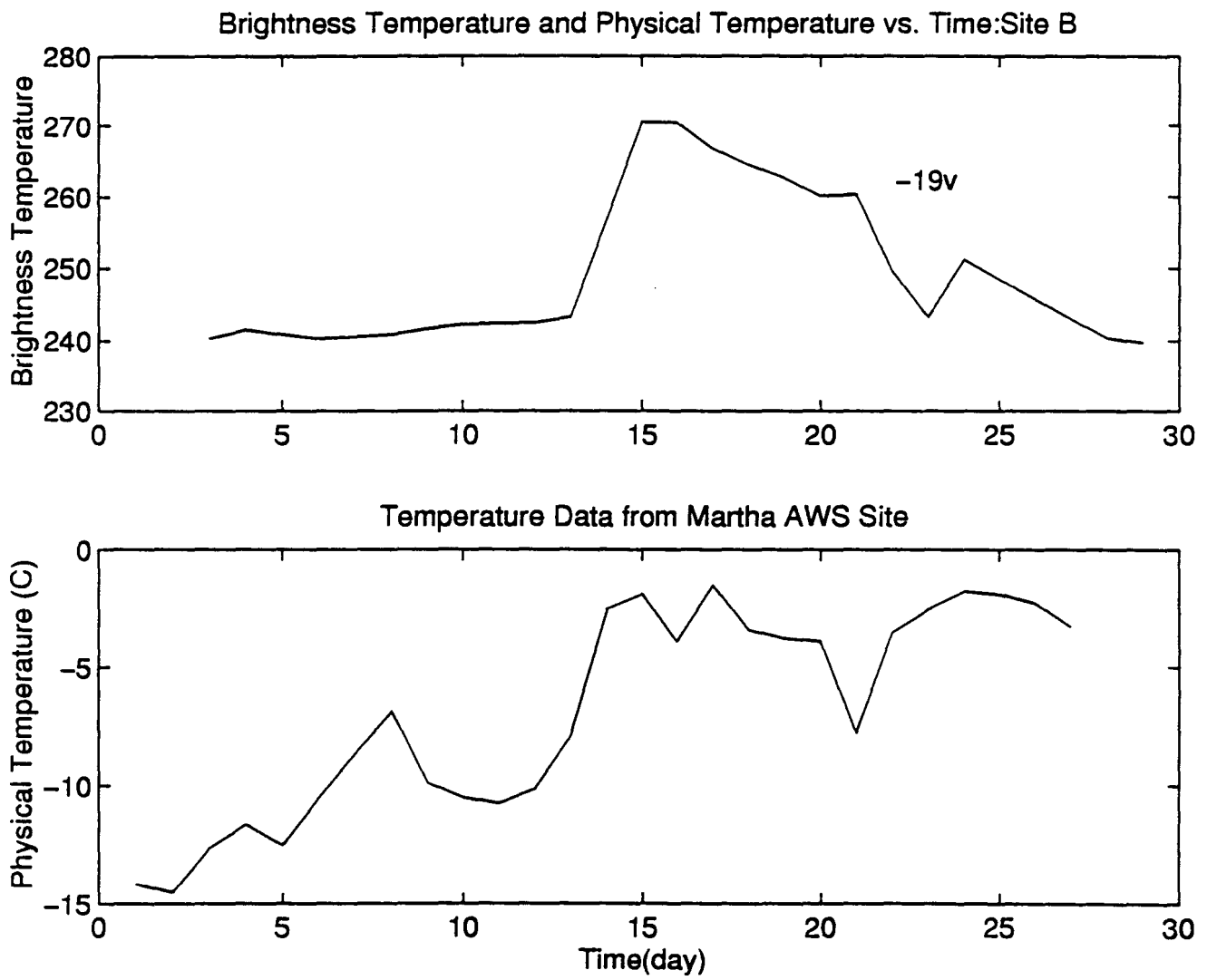


Figure 8. Graph of brightness temperature and physical temperature vs. time of 19GHz.vertical channel, Site B with data from Martha AWS site.

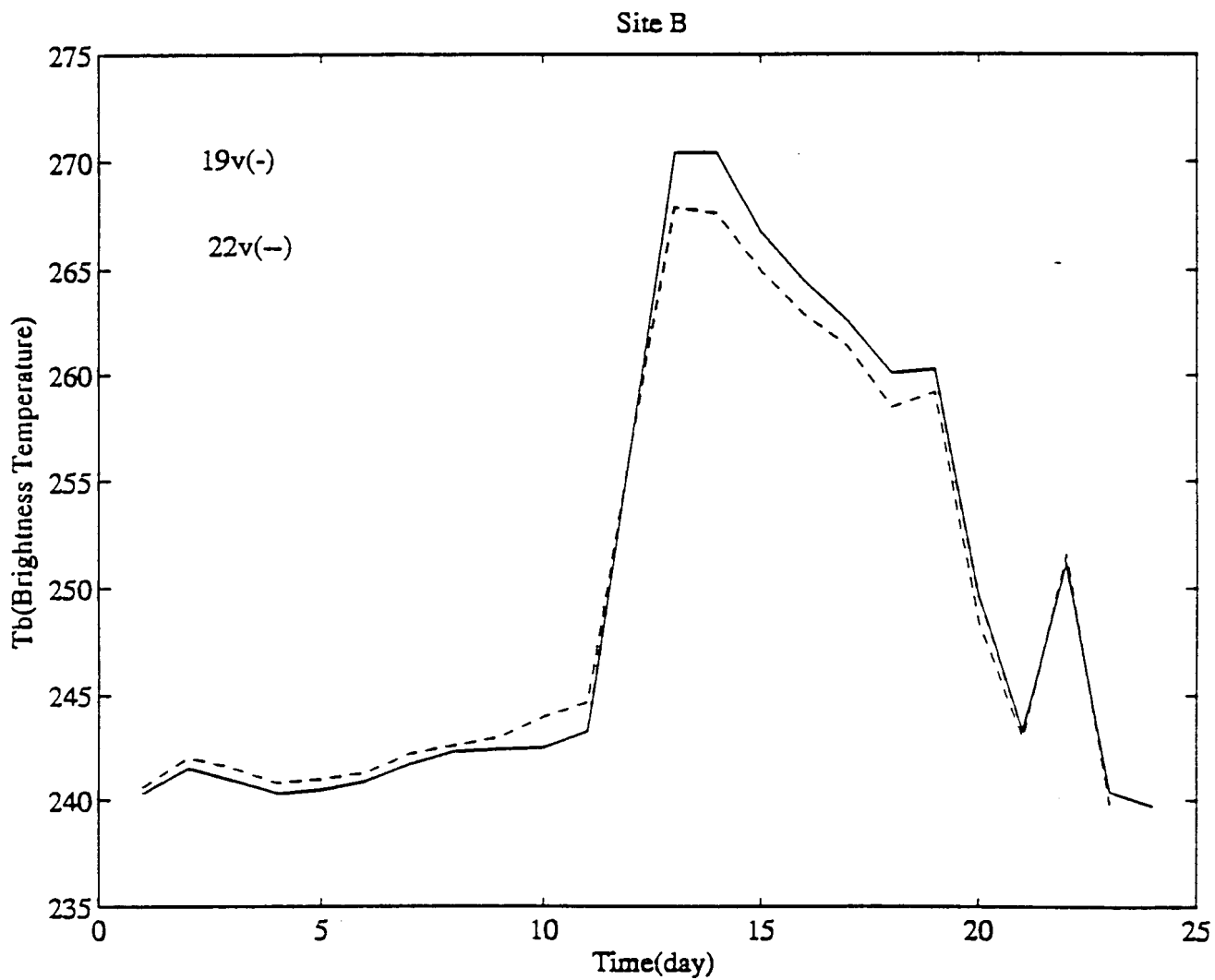


Figure 9. graph of brightness temperature vs. time of 19GHz. vertical and 22GHz. vertical channels at Site B for the month of December 1988.

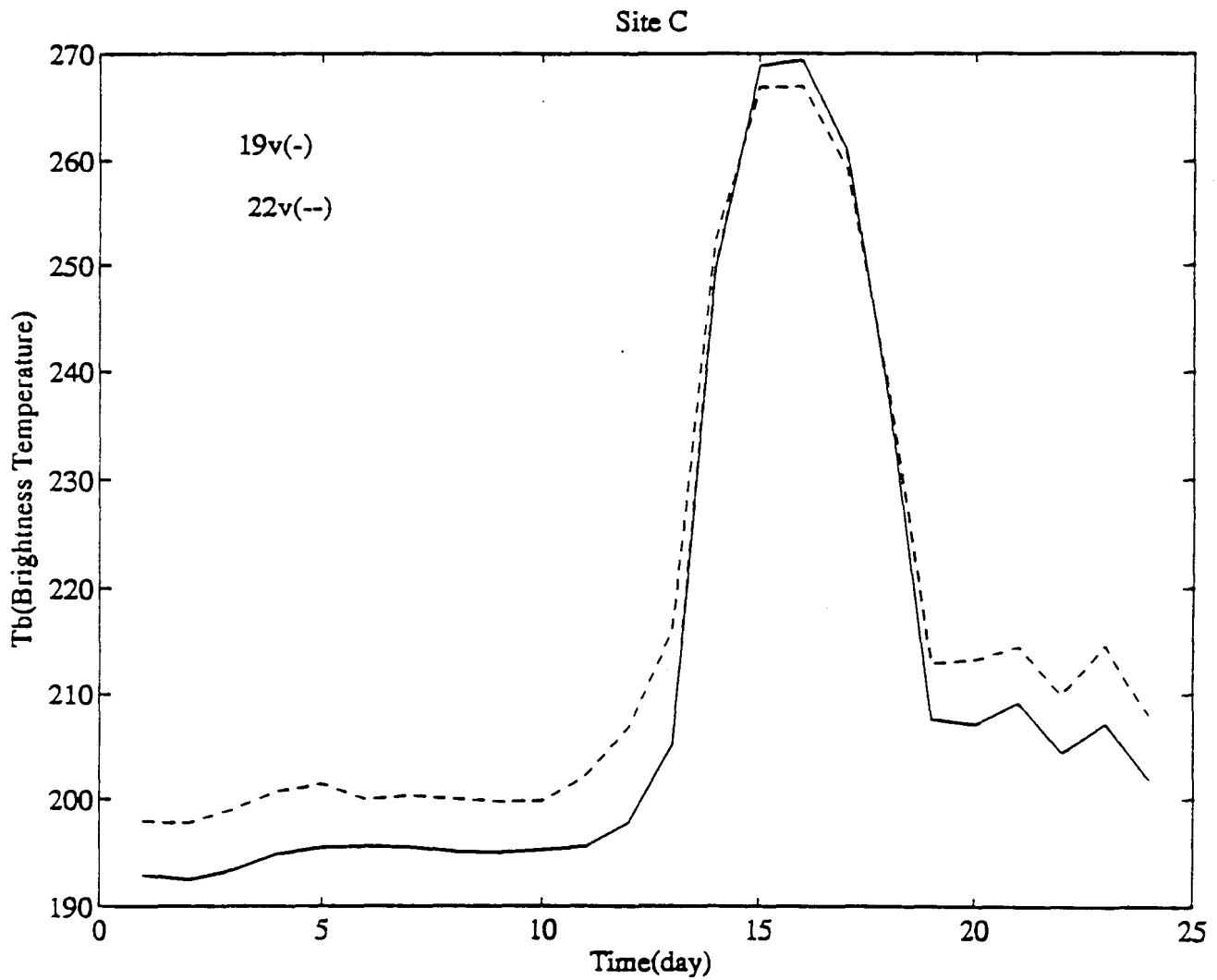


Figure 10. Graph of brightness temperature vs. time of 19GHz. and 22GHz. vertical channels at Site C for the month of December 1988.

similar behavior of these graphs supports the notion that the signature marking the high brightness temperature event was primarily caused by upwelling energy from a wetted snow surface. In the next section, we describe a technique for mapping melt extent emitted from the wetted surface of the ice sheet.

5.0 Cross-Polarization Gradient Ratio Technique

The Cross-Polarized Gradient Ratio or XPGR is a mathematical algorithm designed by Abdalati and Steffen (1995) as a method to determine melt regimes in Greenland. This technique is based on the physical response of polar firn to melting that manifests itself in the passive microwave brightness temperature signal.

Dry snow is essentially composed of ice particles immersed in air or empty pore spaces. Under such conditions, volumetric scattering dominates the received signal (Ulaby et al., 1982). When melting occurs water, which has a higher dielectric constant than air, begins to fill the pore spaces between the grains. This causes scattering and absorption to dominate and subsequently drives the emissivity closer to that of a black body (Matzler and Hueppi, 1989). The XPGR technique takes advantage of these changes in the emissivity through the brightness temperature

signal. As melting occurs in the polar firm the difference between the vertically polarized signal and the horizontally polarized signal becomes larger due to the differences in the bulk reflection coefficient (eq. 2). This scenario has prompted the development of the XPGR algorithm defined as:

$$XPGR = (Tb(19h) - Tb(37v)) / (Tb(19h) + Tb(37v)) \quad (4)$$

where Tb(19h) and Tb(37v) refer to the brightness temperatures of the 19GHz horizontal and the 37GHz vertical channels in the passive microwave data. A single thresholding technique is implemented to determine whether an XPGR values indicates melt. As Abdalati et al. state, this technique takes into consideration atmospheric effects, and the various depths from which the signals propagates. The impacts of these effects are negligible as compared to the role water plays in the overall signal.

5.1 XPGR Method Applied to Antarctica

The XPGR method is easily adaptable for analysis on seasonal, monthly, weekly, or daily time scales, but also to other geographic locations (Abdalati and Steffen,1995). The XPGR was applied initially to brightness temperature data collected over locations which offered

information about intermittent melt events in West Antarctica. The determination of a melt threshold value for these sites was accomplished through the application of the XPGR algorithm to annual brightness temperature data at these sites. First the XPGR was used to calculate a base XPGR melt threshold value. This base melt value was derived from:

$$\text{XPGR}(\text{base}) = (\langle \text{Tb19h} \rangle - \langle \text{Tb37v} \rangle) / (\langle \text{Tb19h} \rangle + \langle \text{Tb37v} \rangle) \quad (5)$$

where $\langle \text{Tb19h} \rangle$ and $\langle \text{Tb37v} \rangle$ refer to the mean brightness temperature calculated from the Antarctic summer brightness temperatures between mid November and January of the next year from 1988 through 1991. From this value, a melt threshold was defined as half the base XPGR threshold. The motivation for this was to determine a value for the melt threshold that would be sufficiently less negative than the base XPGR and so as not to include the general increase in the Tb signal due to the increase in physical temperature characteristic for the Antarctic summer.

$$\text{XPGR}(\text{Melt Threshold}) = 1/2 (\text{XPGR}(\text{base})) \quad (6)$$

Figures 11 and 12 show 1988-1991 time series graphs of XPGR vs. Time for Sites C and B respectively. In these graphs we can detect intervals of time when, according to our method, melt occurs. Notice that at both sites the December 1988 event evident in the passive microwave data is identified as a prominent melt signature according to our melt threshold scheme. Note the difference between the melt threshold values for both sites. This has led us to believe that the XPGR melt threshold value is site specific, as discussed in more detail later.

6.0 Results Section

The XPGR algorithm was applied to the sites listed in Table I. Figures 13 through 16 plot XPGR vs. Time at Site C from 1988 to 1991. Each graph shows the XPGR base and melt threshold values calculated for this site according to the melt determining method we used. The December 1988 melt event is evident in Figure 13 as an obvious spike extending beyond the melt threshold value which was fixed at -0.0587 . Figure 14 illustrates that according to our melt determining scheme, there was no melting during 1989. Figure 15. shows a sharp spike during the months of November and December of 1990 but the spike does not exceed the melt threshold. Though an obvious warming event occurred

XPGR vs. Time:Site C 1988-1991 (Lampkin Threshold)

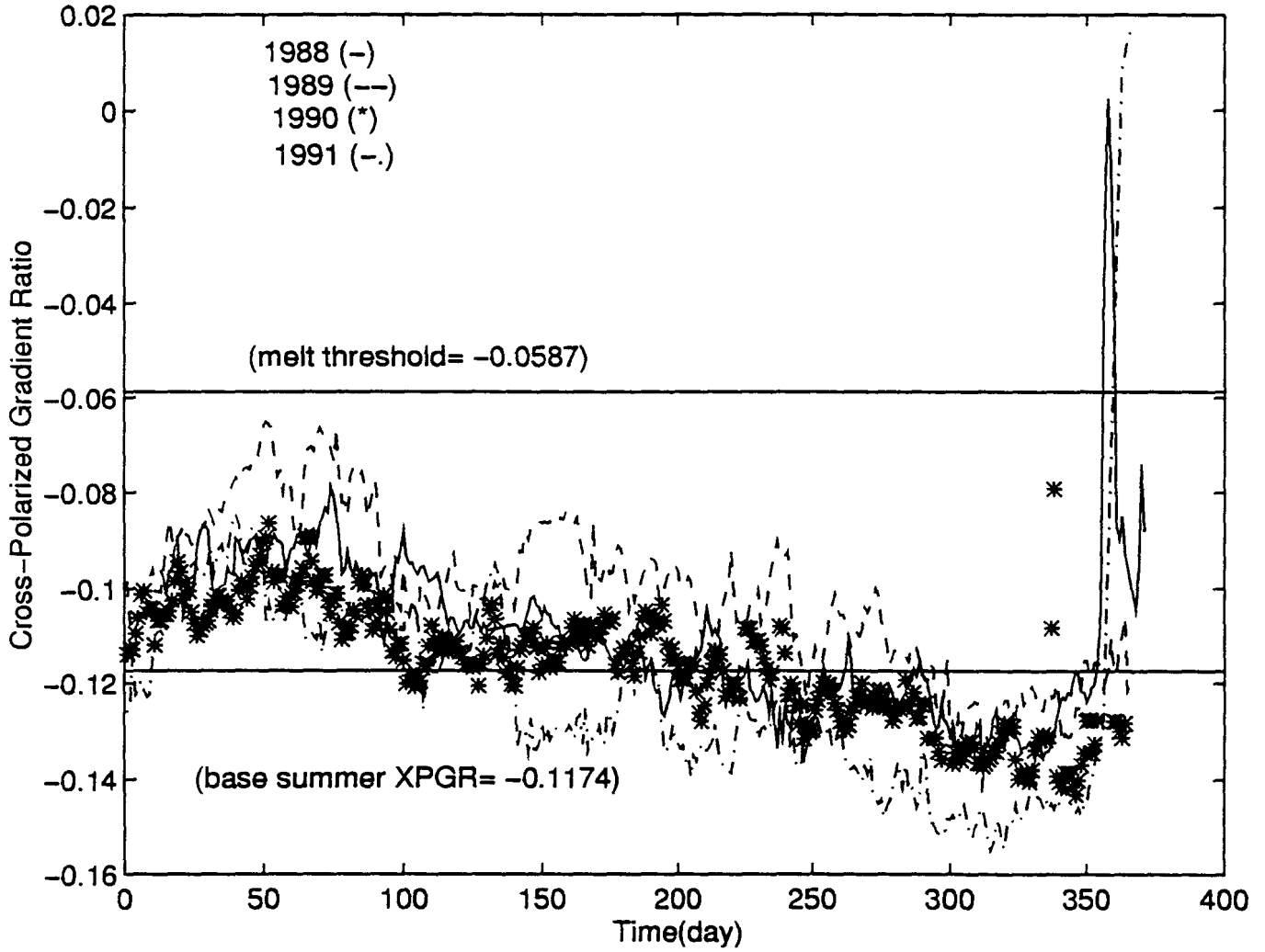


Figure 11. Composite graph of XPGR vs. time at Site C from 1988-1991 showing melt threshold and base summer XPGR values.

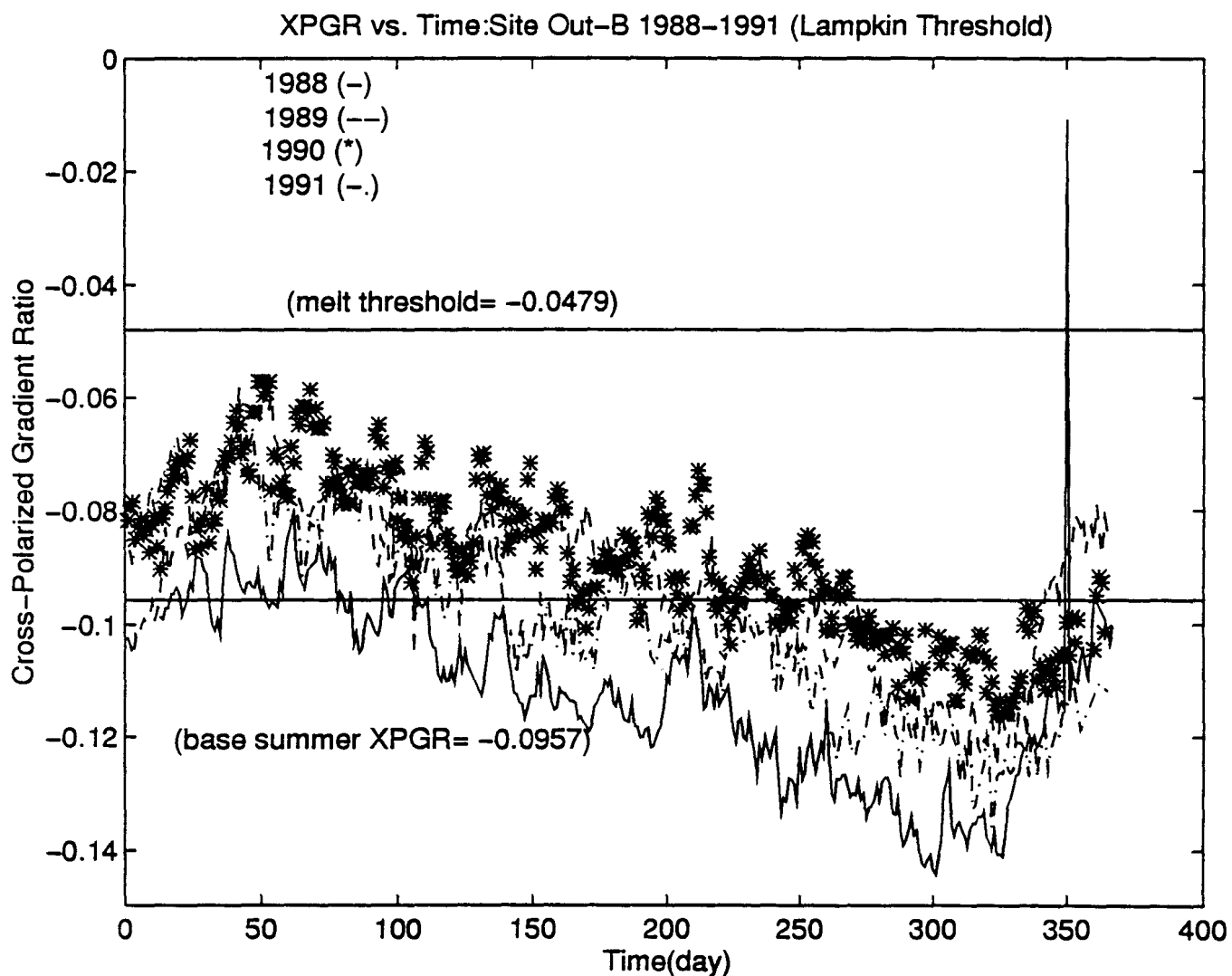


Figure 12. Composite graph of XPGR vs. time at Site Out-B from 1988-1991 showing melt threshold and base summer XPGR values.

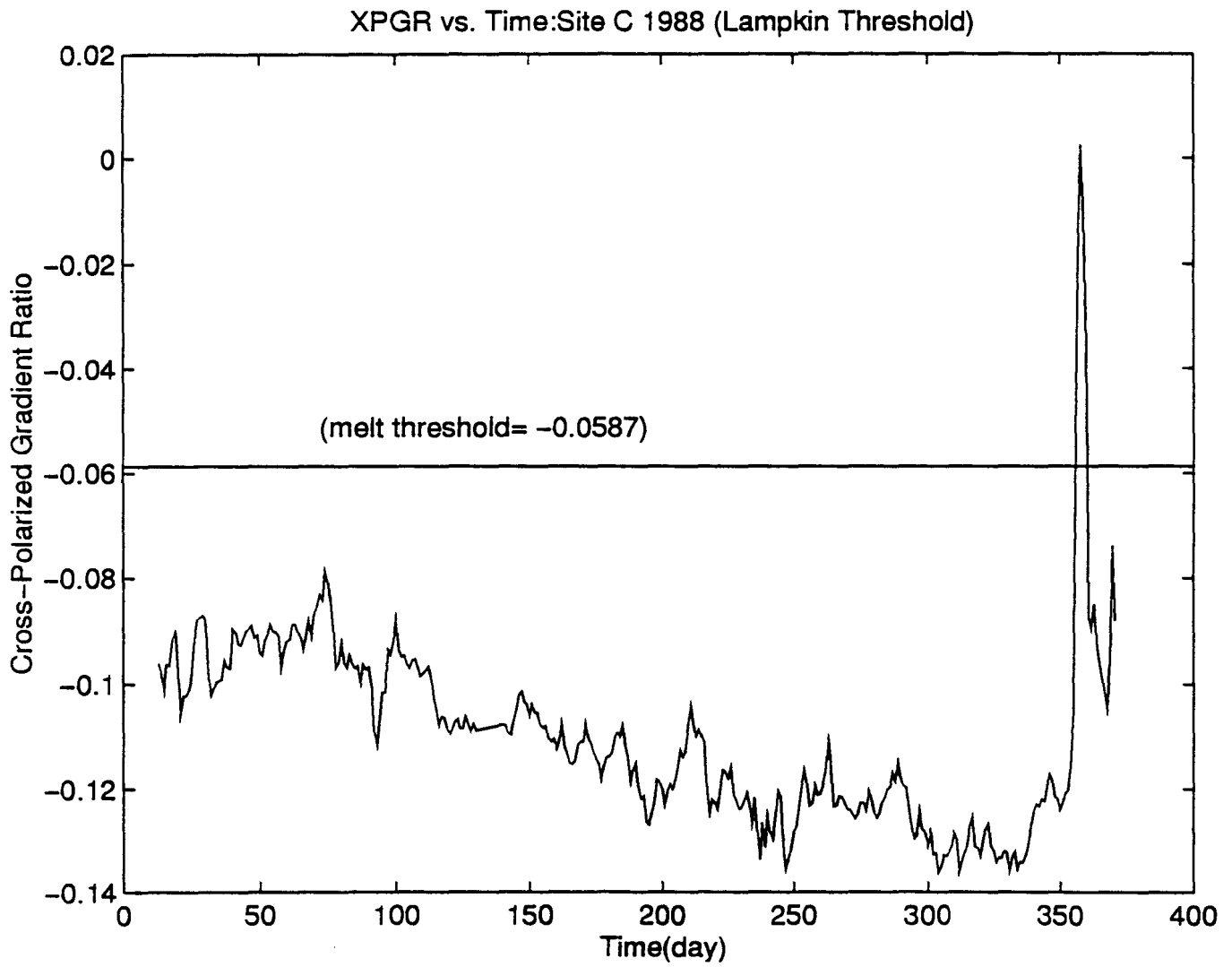


Figure 13. Graph of XPGR vs. time at Site C for the year of 1988.

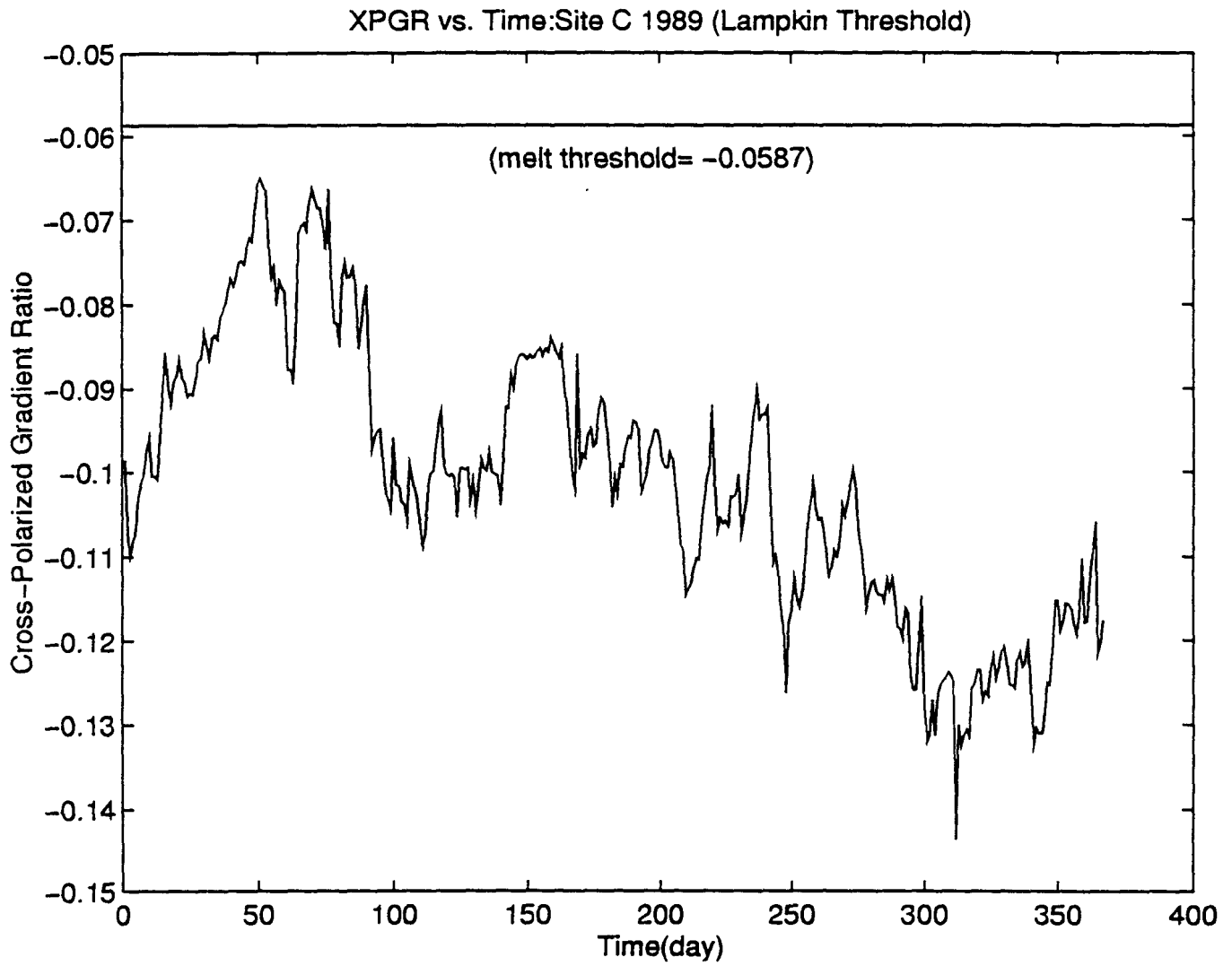


Figure 14. Graph of XPGR vs time at Site C for the year of 1989.

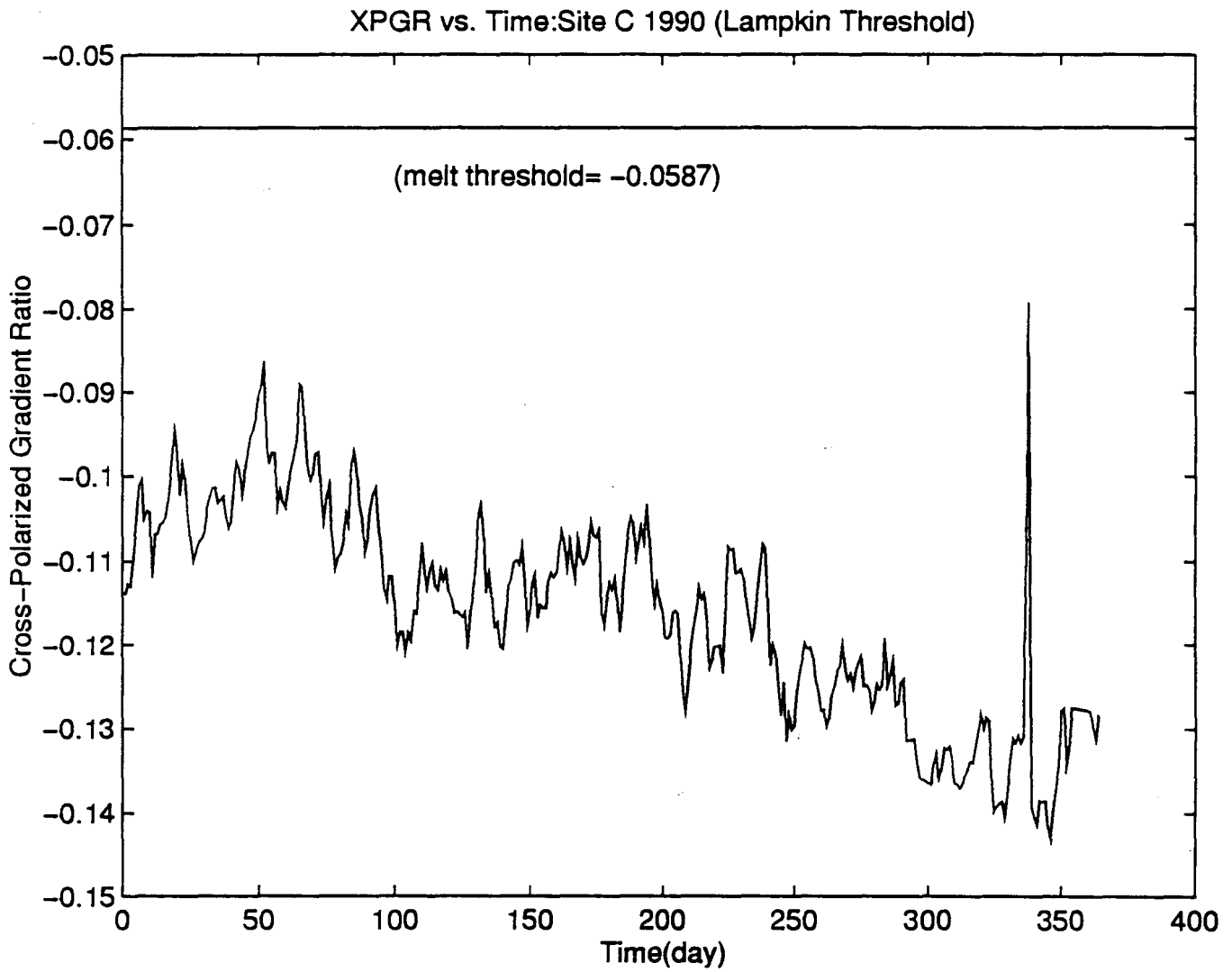


Figure 15. Graph of XPGR vs. time at Site C for the year of 1990.

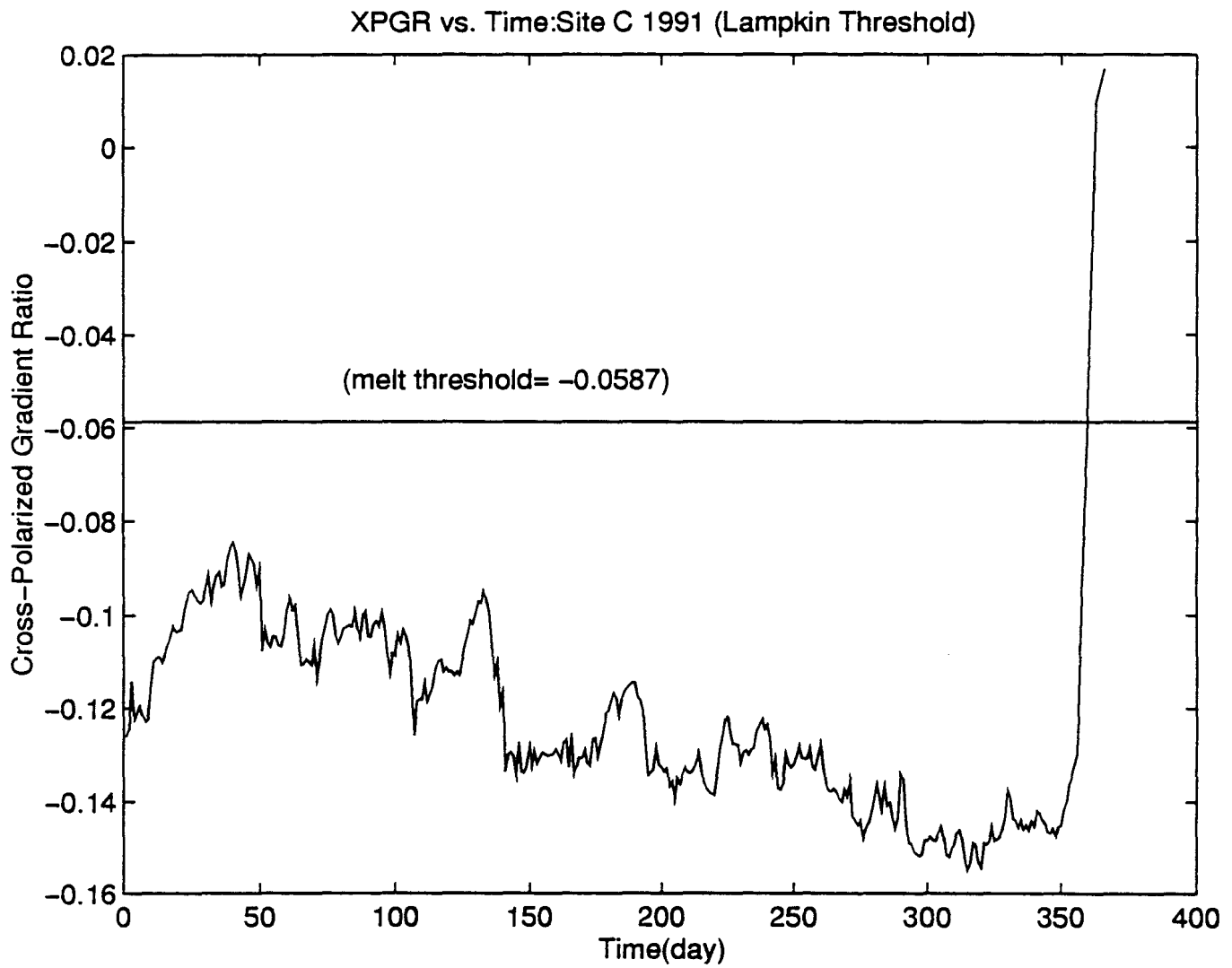


Figure 16. Graph of XPGR vs. time at Site C for the year of 1991.

during that Antarctic summer it was not sufficiently warm enough to cause surface melt. Lastly, Figure 16. exhibits an obvious melt spike at the end of 1991.

Figures 17 through 36 are time series plots of XPGR from 1988 through 1991 for sites B, Out-B, D, E, and F. Figure 18 shows an unusual trend during day 70. This has been attributed to random error in the original data set. The melt threshold for all sites is listed in Table III. According to the Lampkin Threshold, melt events at Site B, C and D occurred in 1988 and 1991. Site Out-B shows a melt event in summer of 1988, whereas Site E show melt in the summer of 1991 only. Site F is the only site that does not exhibit any melt events according to our melt determining technique.

XPGR melt thresholds for the selected sites are all plotted in Figure 37. The difference in melt threshold has lead us to believe that the XPGR melt thresholds are site specific. Site B has the least negative melt threshold (see table III). The order continues with Site Out-B plotted as the next highest melt value, Site F, and Site D plotted relatively close, next is Site C with Site E being the lowest melt value. To account for these results, we speculate that there may be a relationship between elevation and XPGR. Elevation and XPGR melt threshold values taken from Table III are plotted in figure 38. In this figure, of XPGR vs. Elevation the distribution of the plots suggest that the relationship between XPGR and

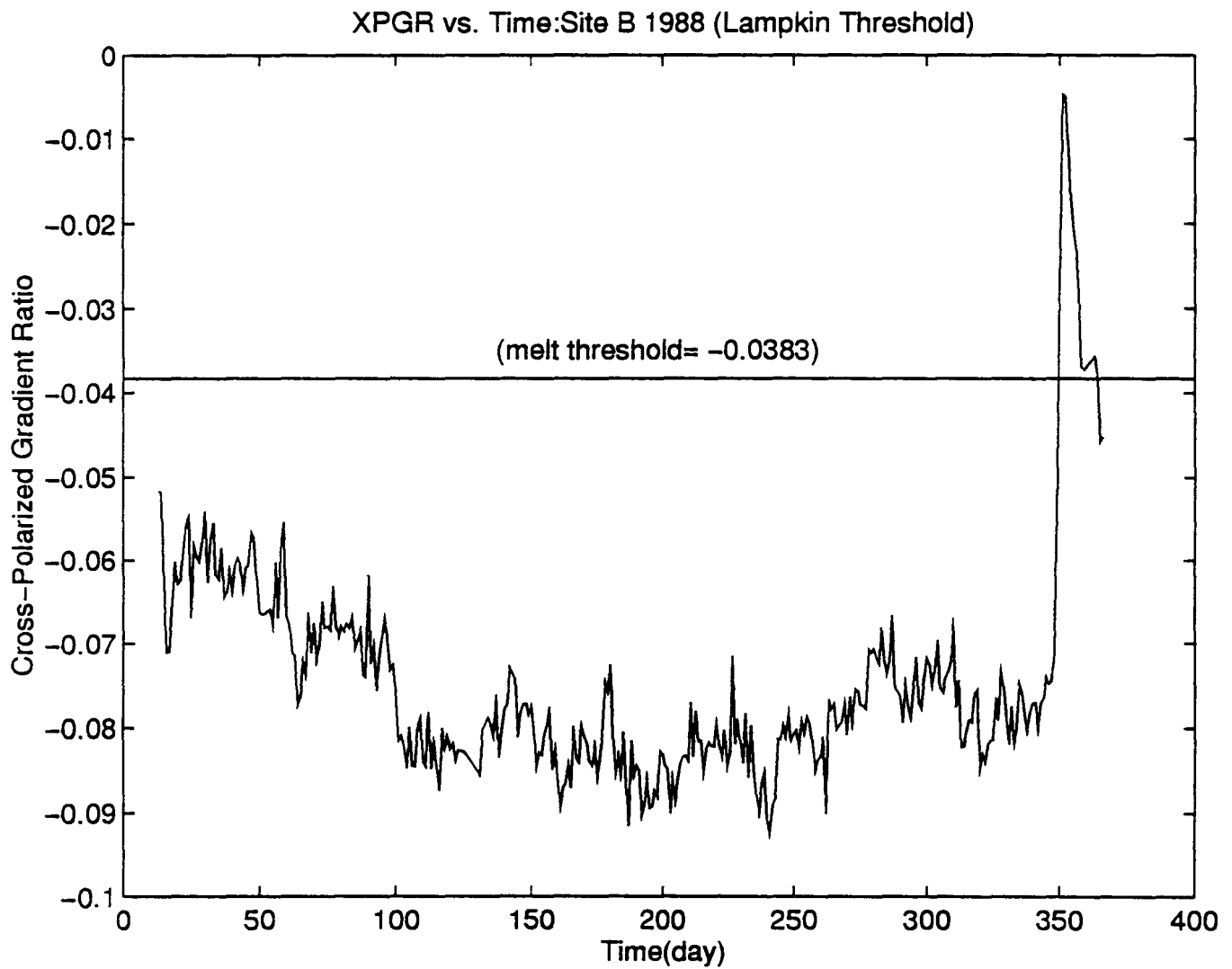


Figure 17. Graph of XPGR vs. time at Site B for the year of 1988.

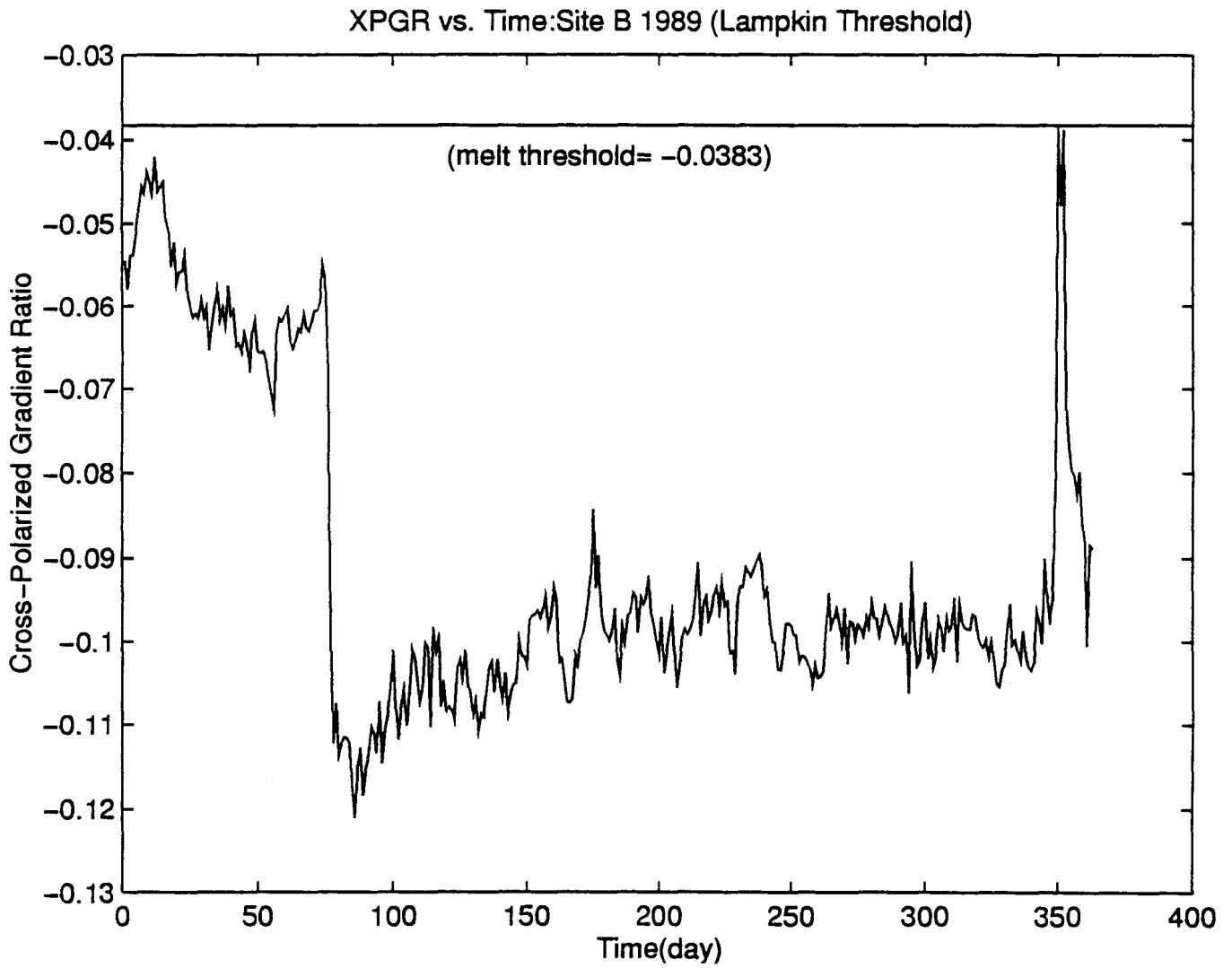


Figure 18. Graph of XPGR vs. time at Site B for the year of 1989.

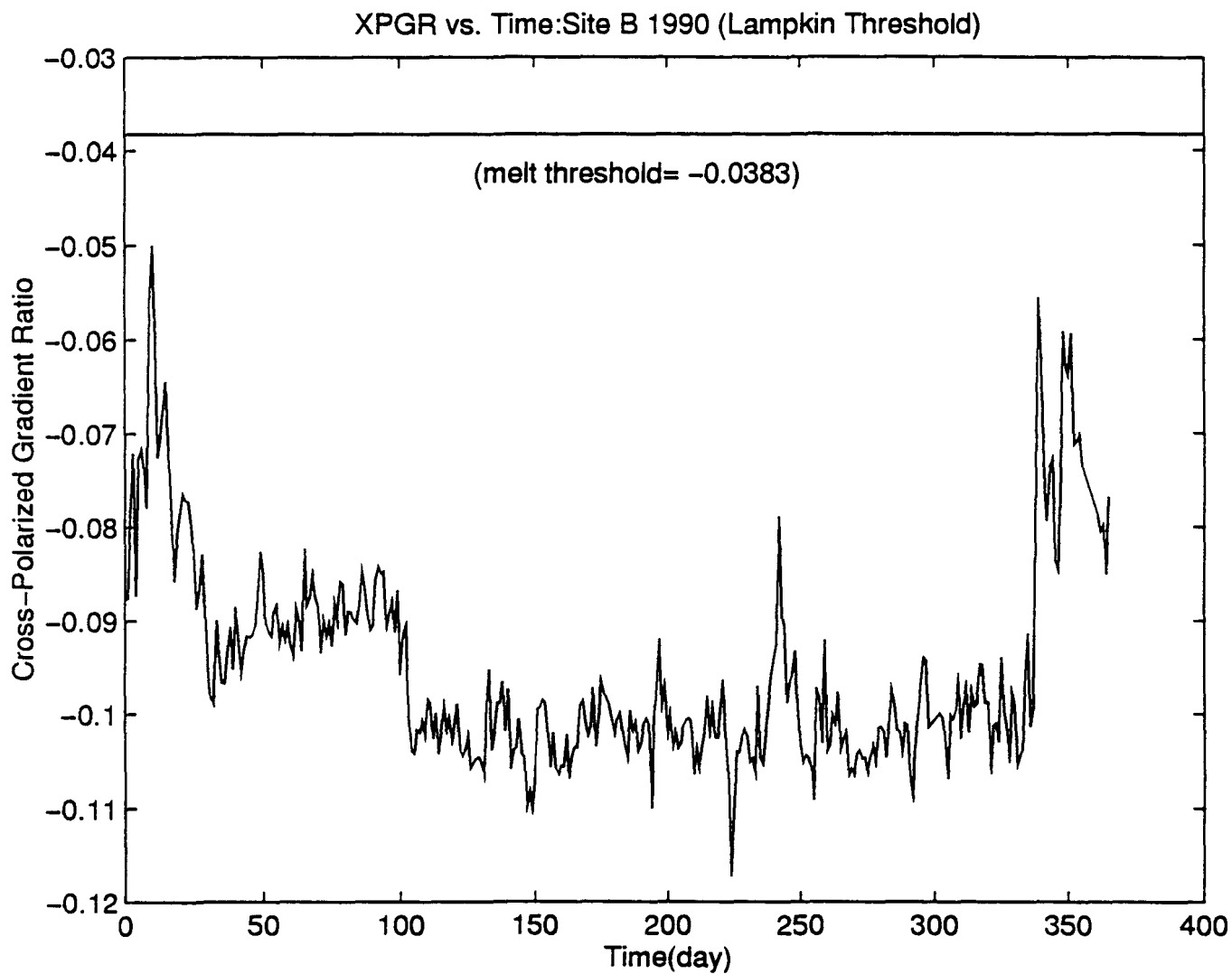


Figure 19. Graph of XPGR vs. time at Site B for the year of 1990.

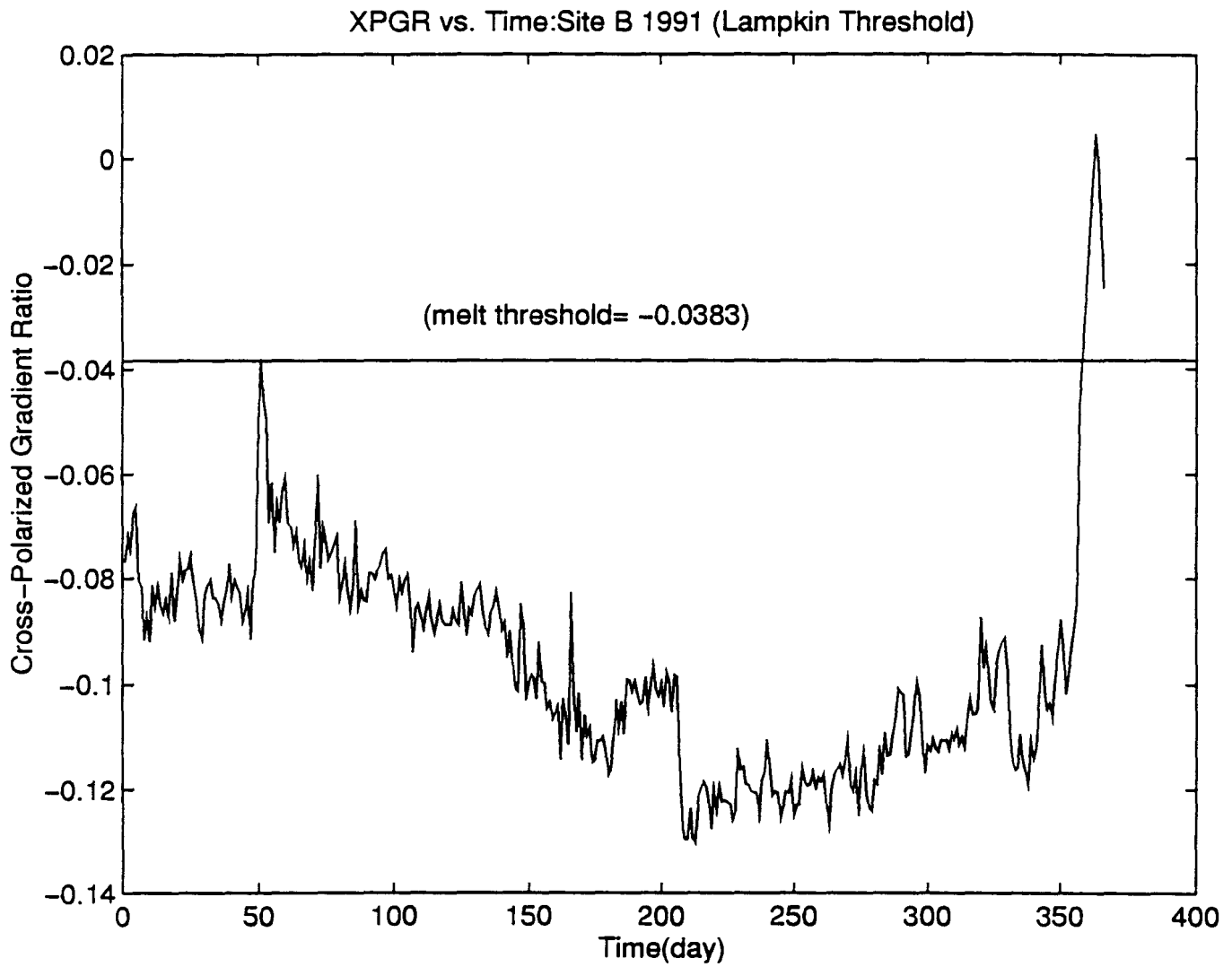


Figure 20 Graph of XPGR vs. time at Site B for the year of 1991.

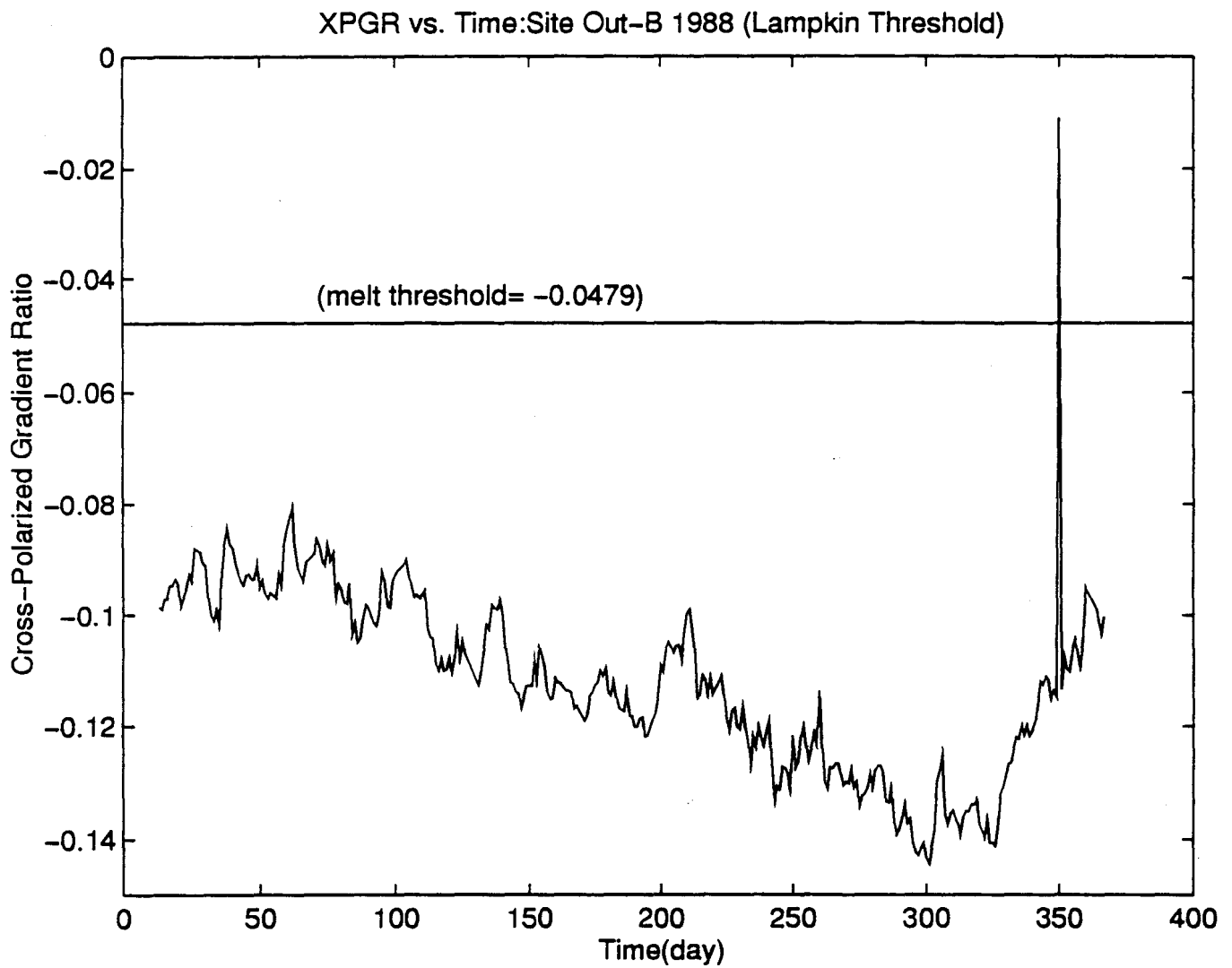


Figure 21. Graph of XPGR vs time at Site Out-B for the year of 1988.

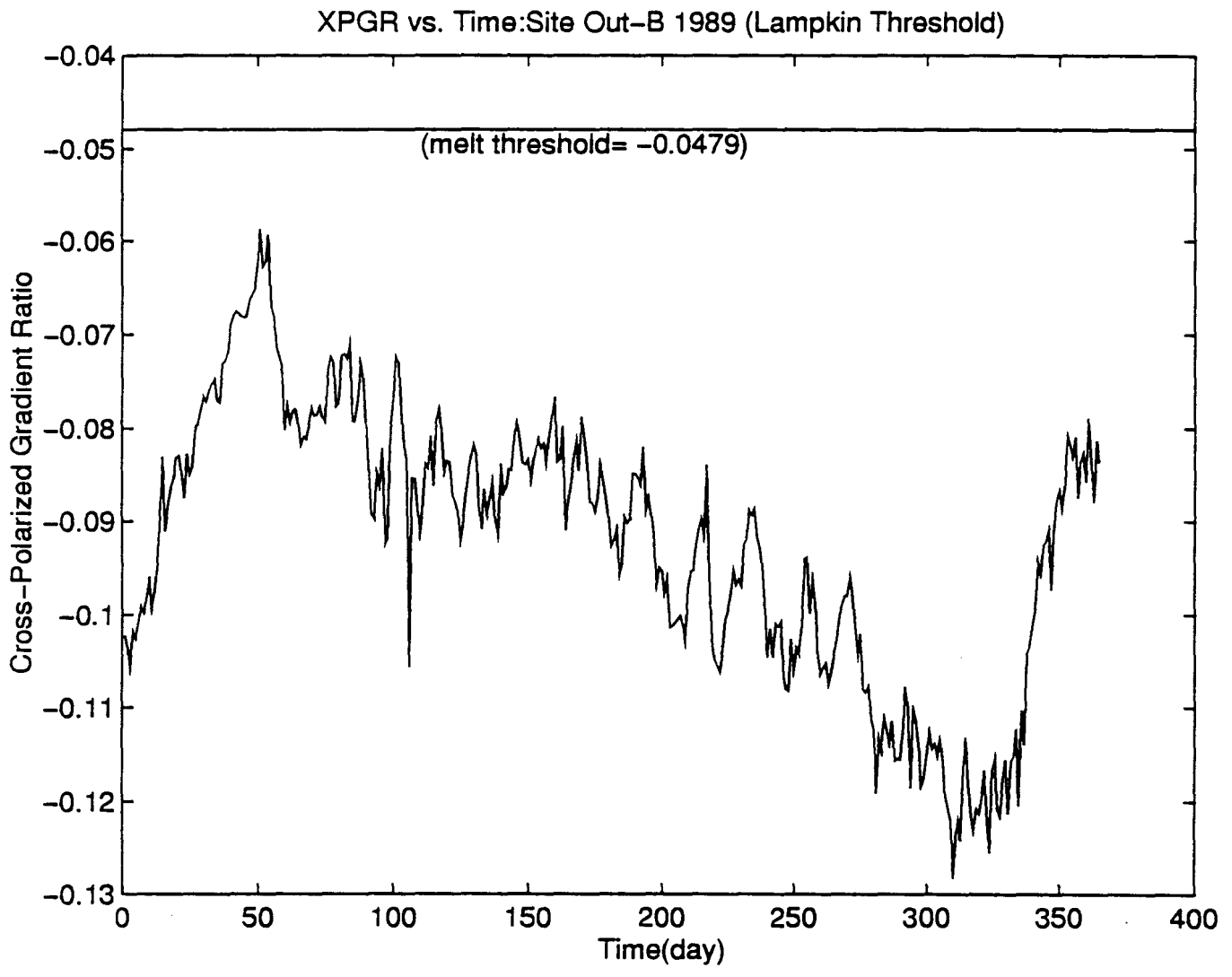


Figure 22. Graph of XPGR vs. time at Site Out-B for the year of 1989.

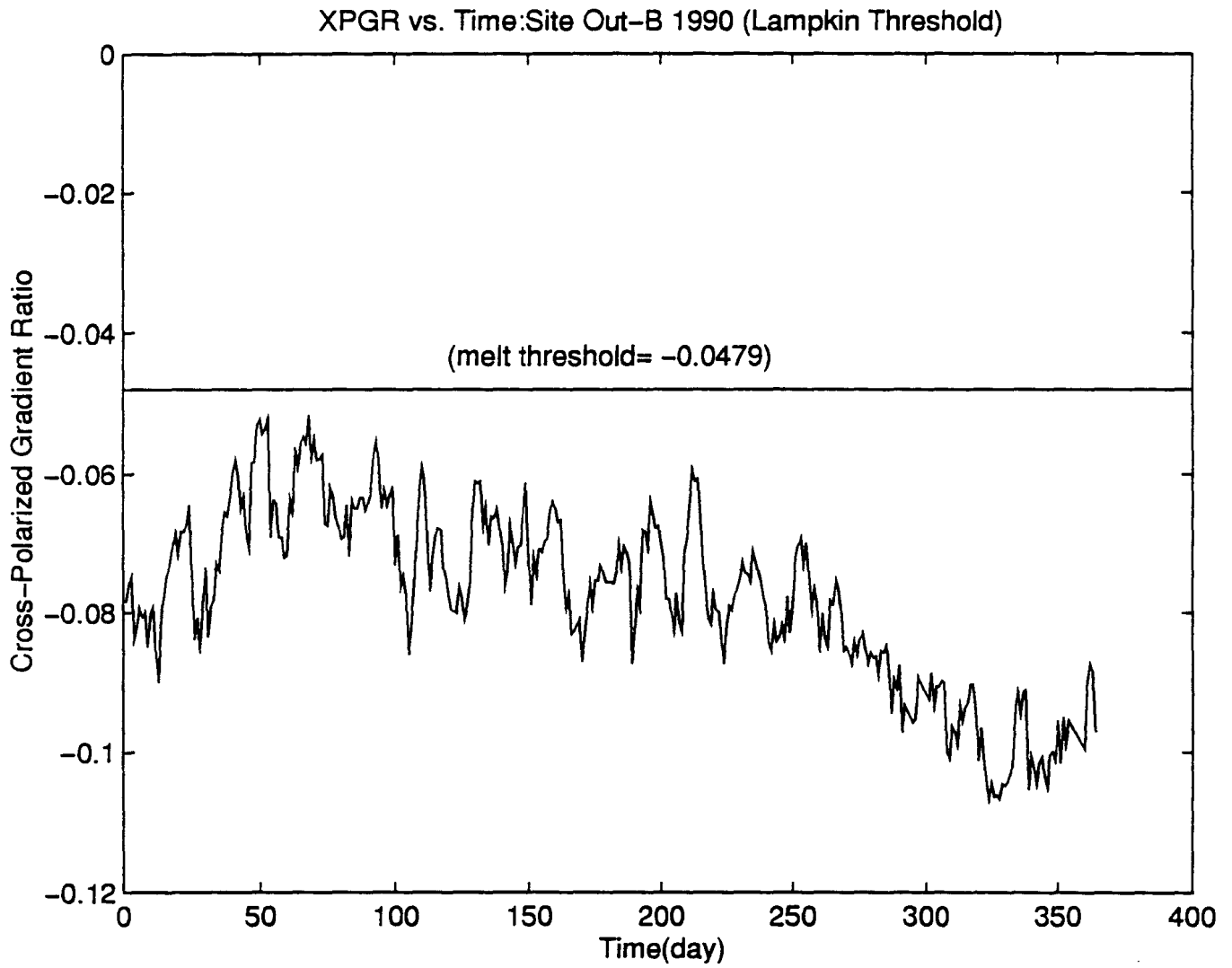


Figure 23. Graph of XPGR vs. time at Site Out-B for the year of 1990.

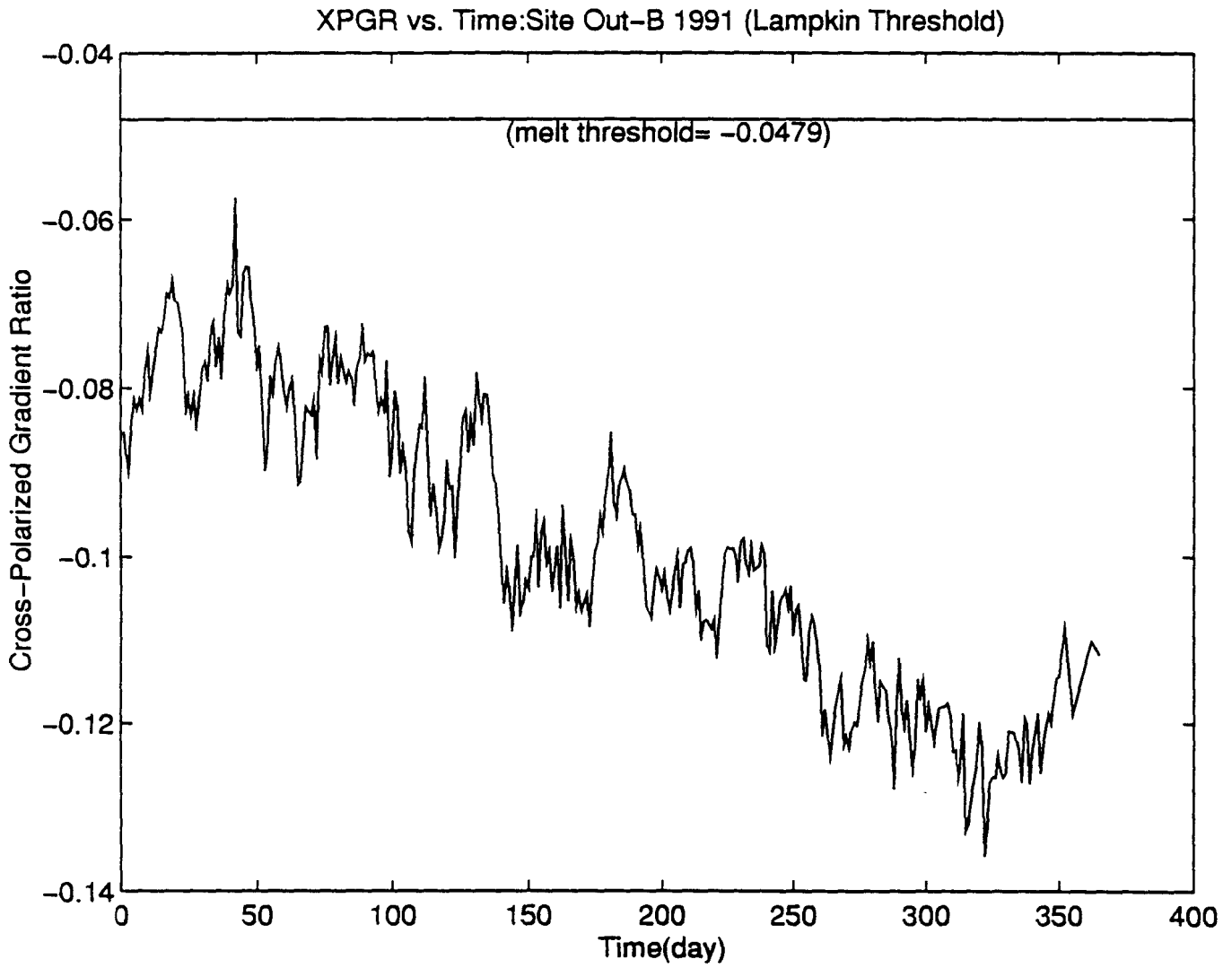


Figure 24. Graph of XPGR vs. time at Site Out-B for the year of 1991.

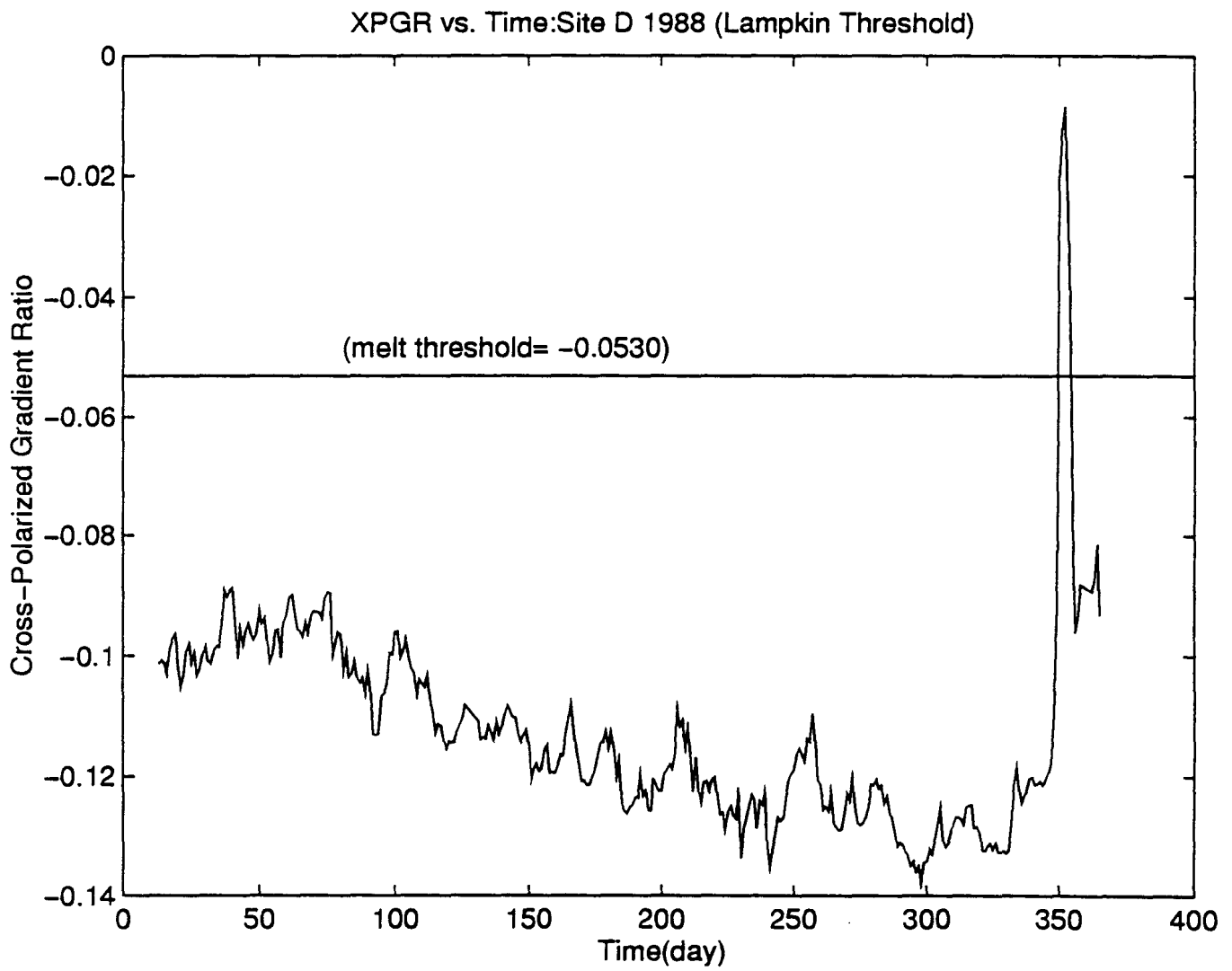


Figure 25. Graph of XPGR vs. time at Site D for the year of 1988.

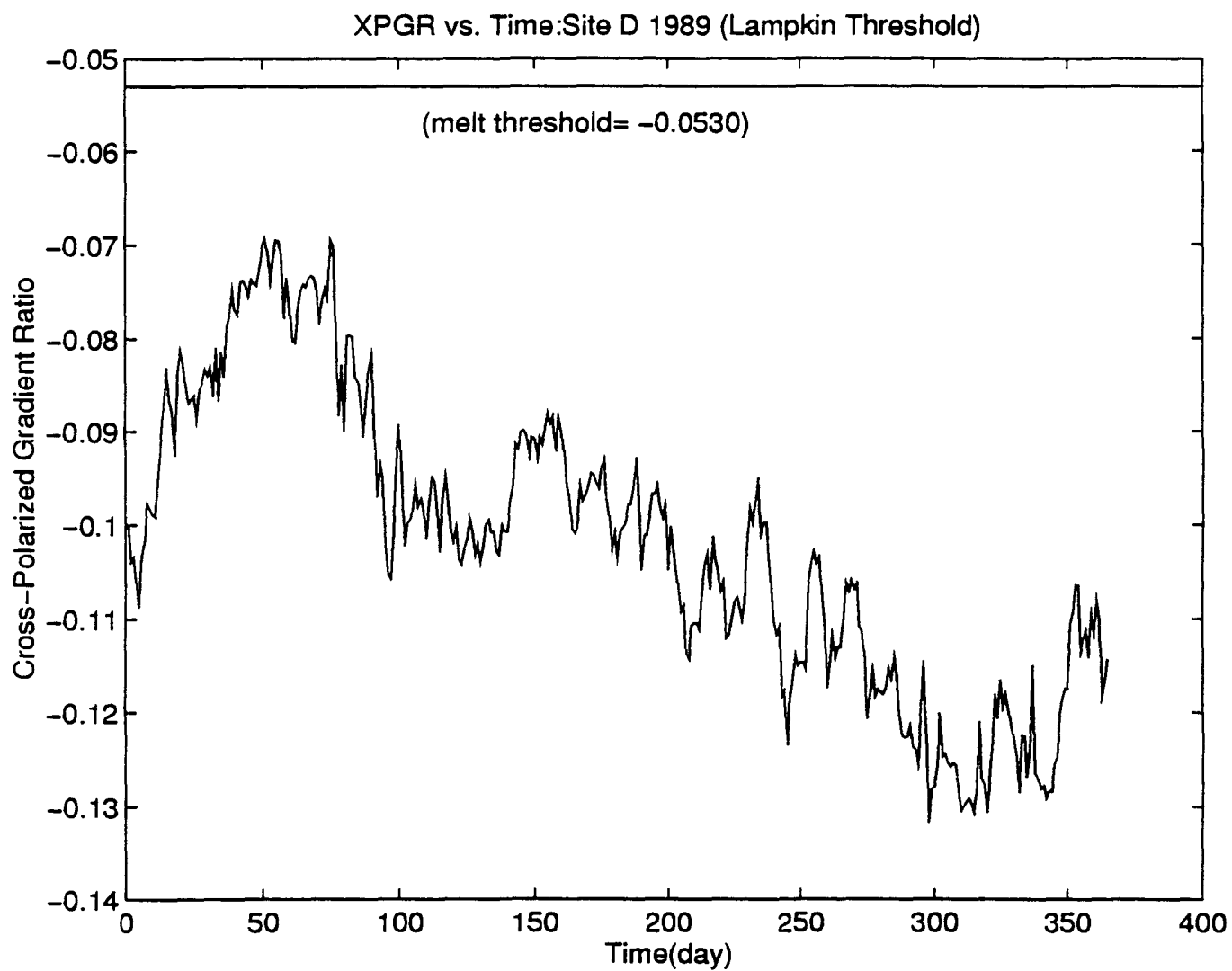


Figure 26. Graph of XPGR vs. time at Site D for the year of 1989.

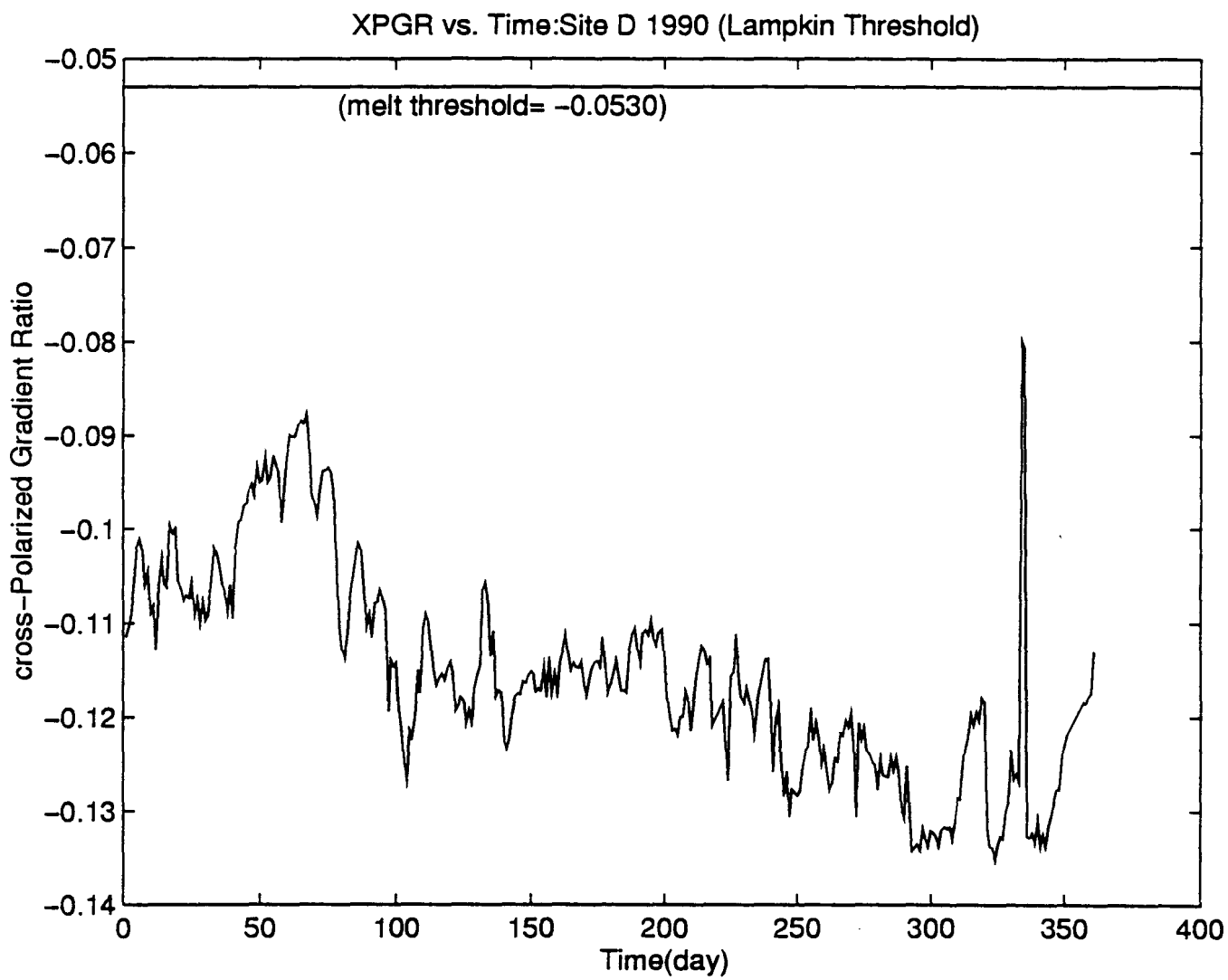


Figure 27. Graph of XPGR vs. time at Site D for the year of 1990.

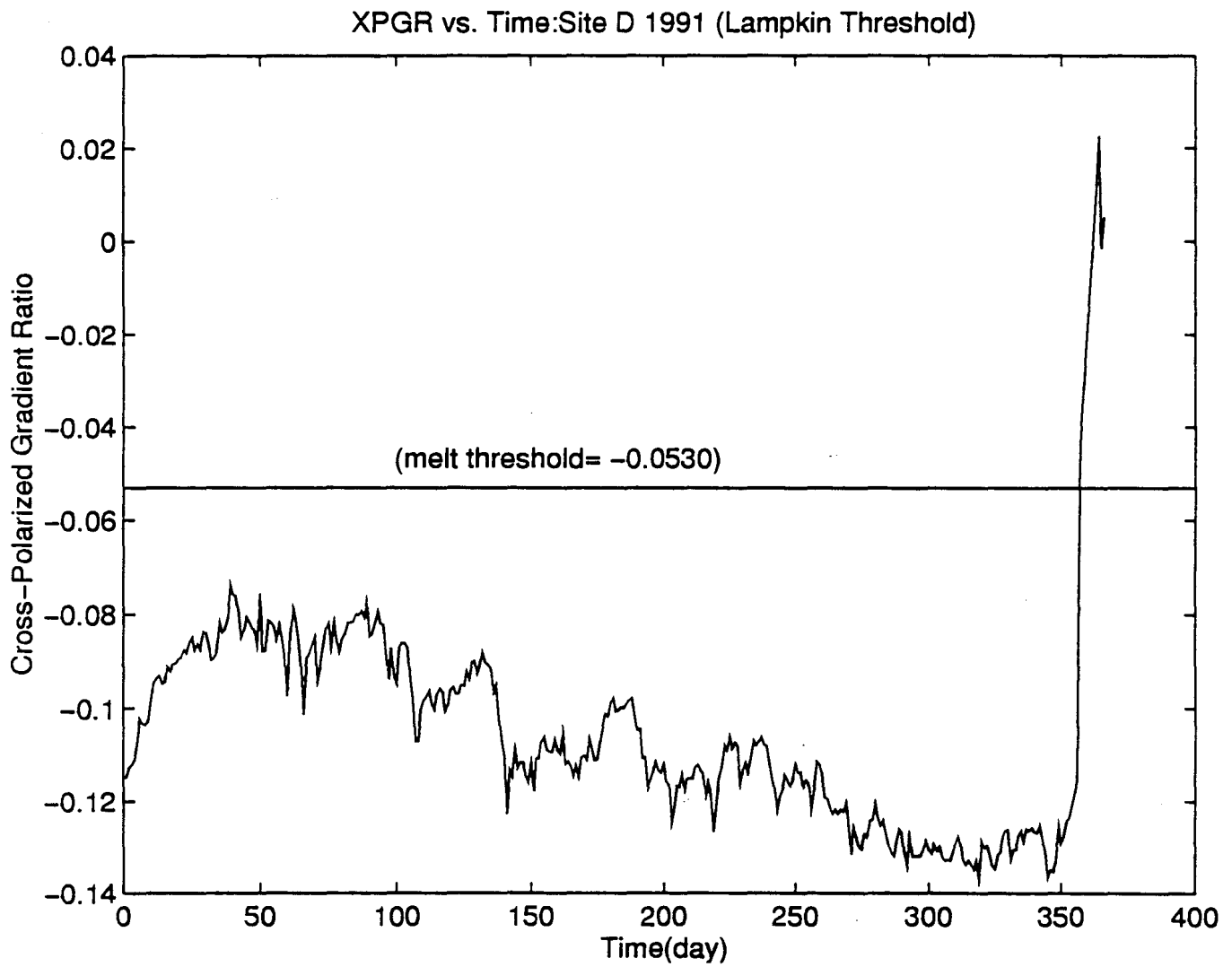


Figure 28. Graph of XPGR vs. time at Site D for the year of 1991.

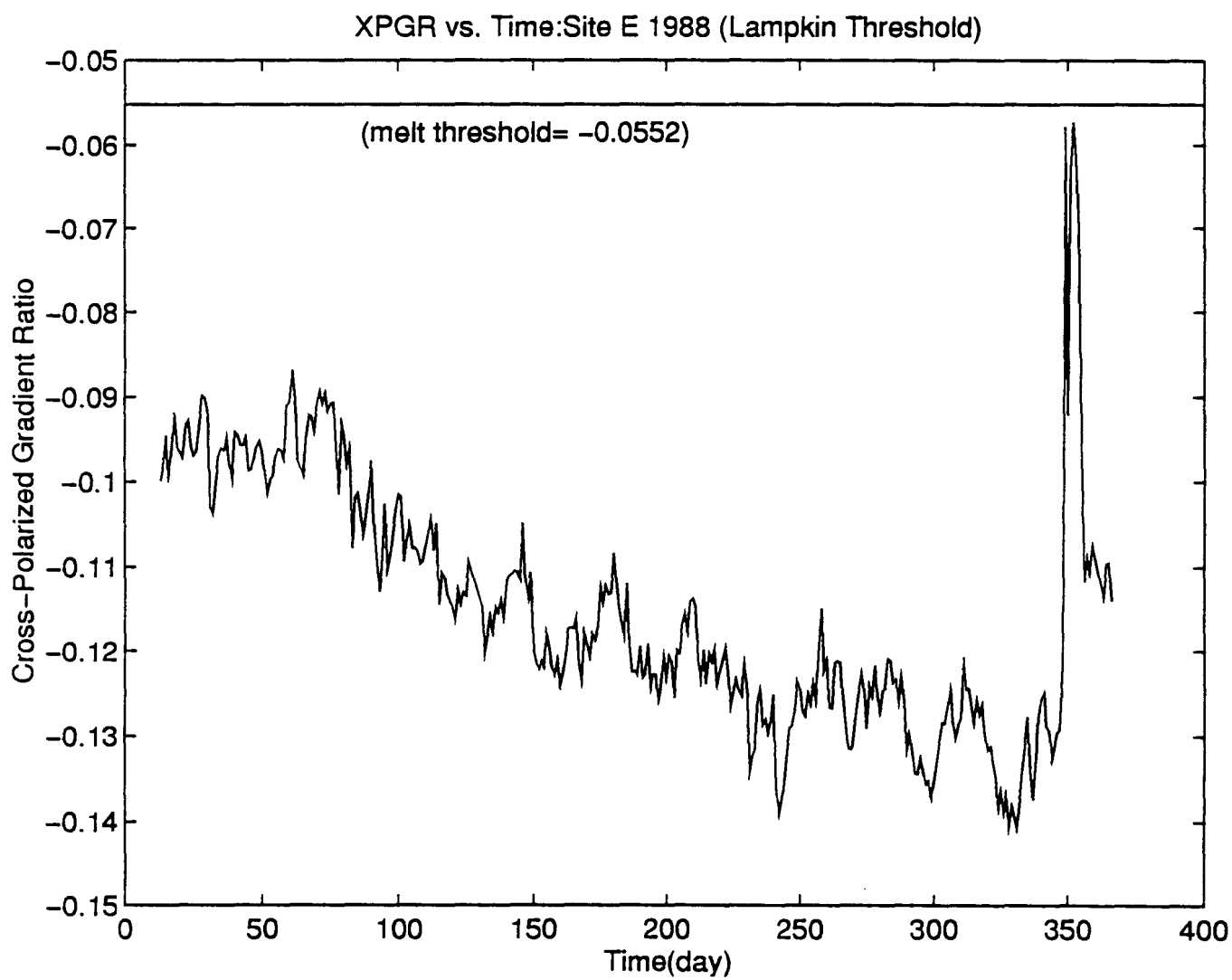


Figure 29. Graph of XPGR vs. time at Site E for the year of 1988.

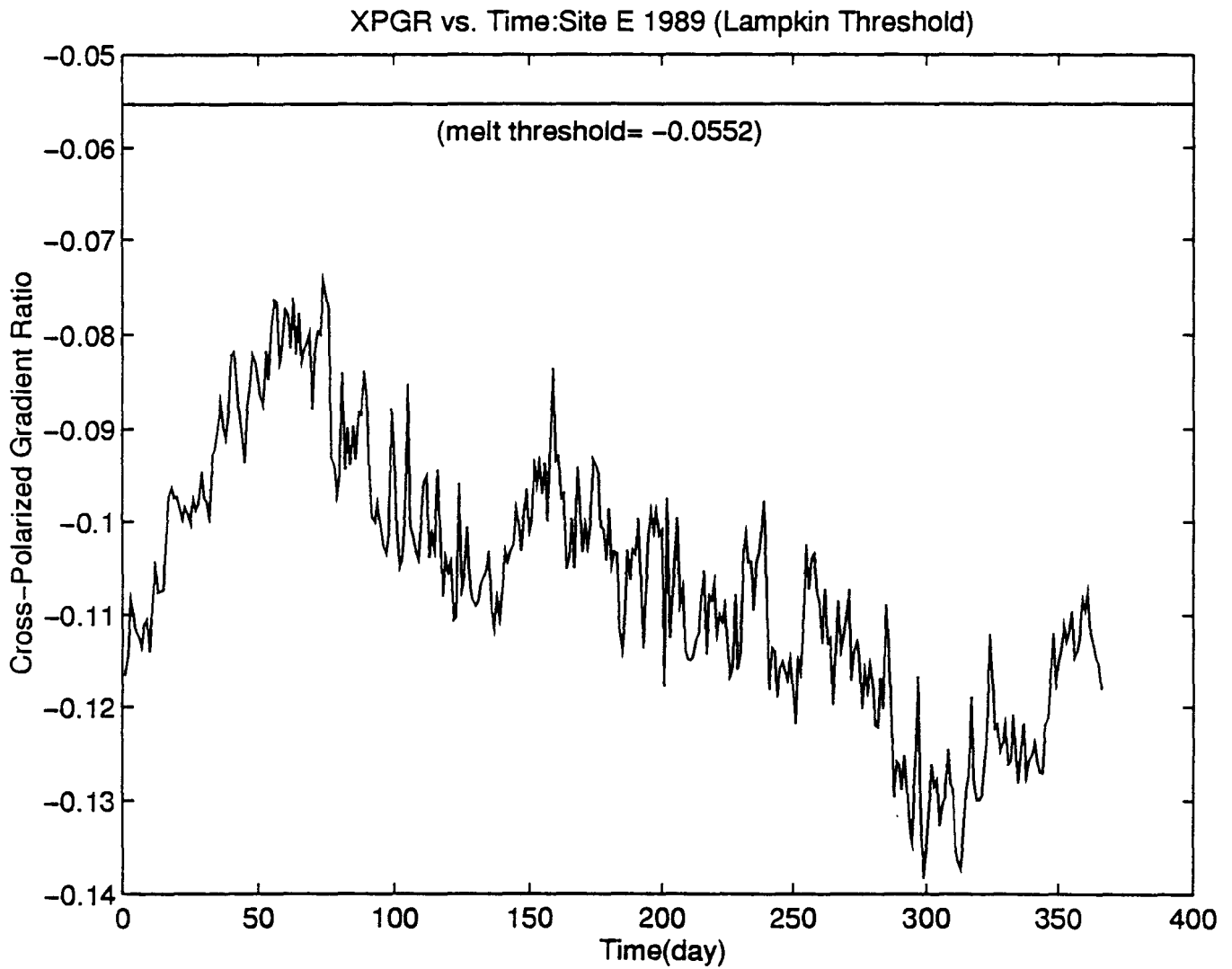


Figure 30. Graph of XPGR vs. time at Site E for the year of 1989.

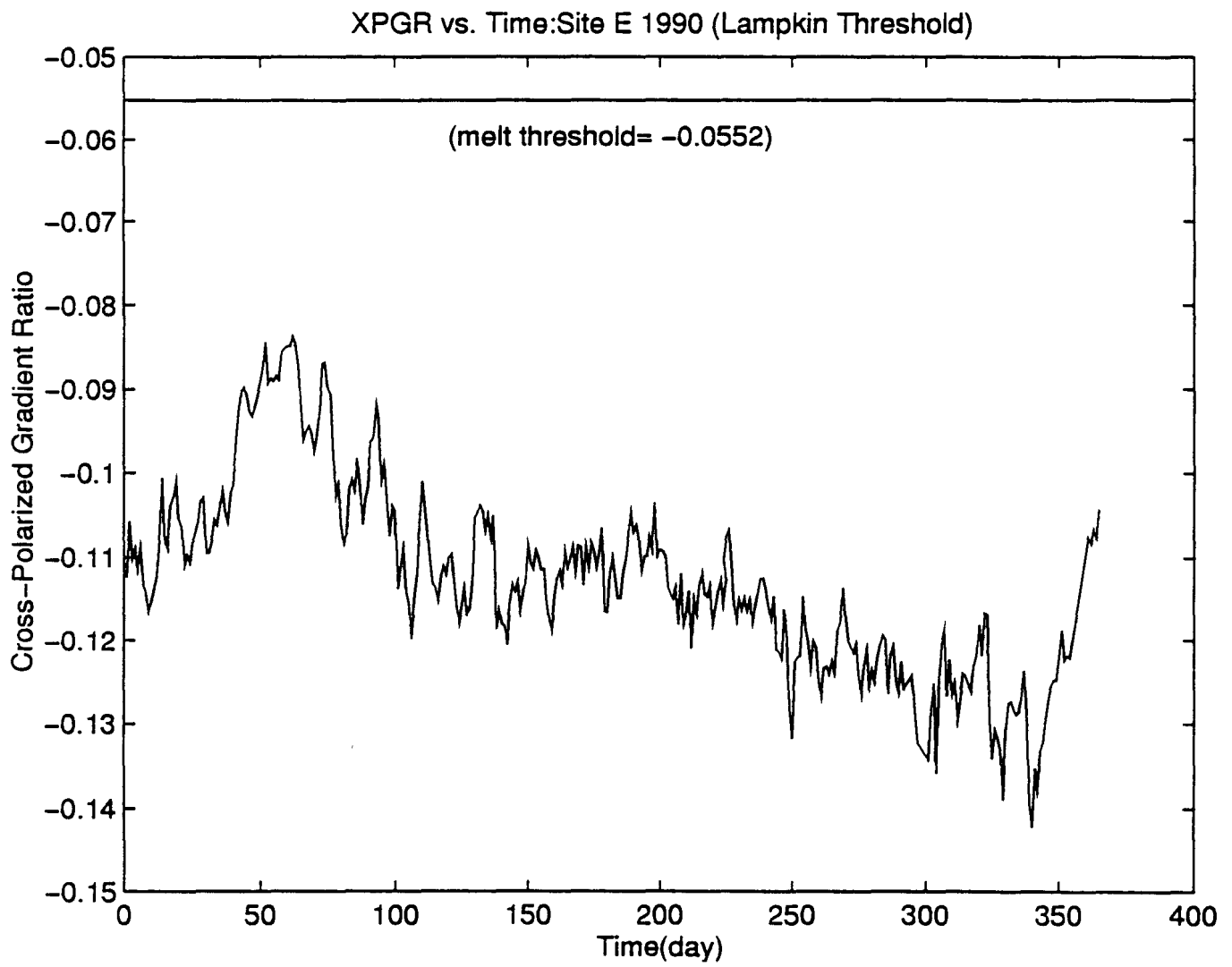


Figure 31. Graph of XPGR vs. time at Site E for the year of 1990.

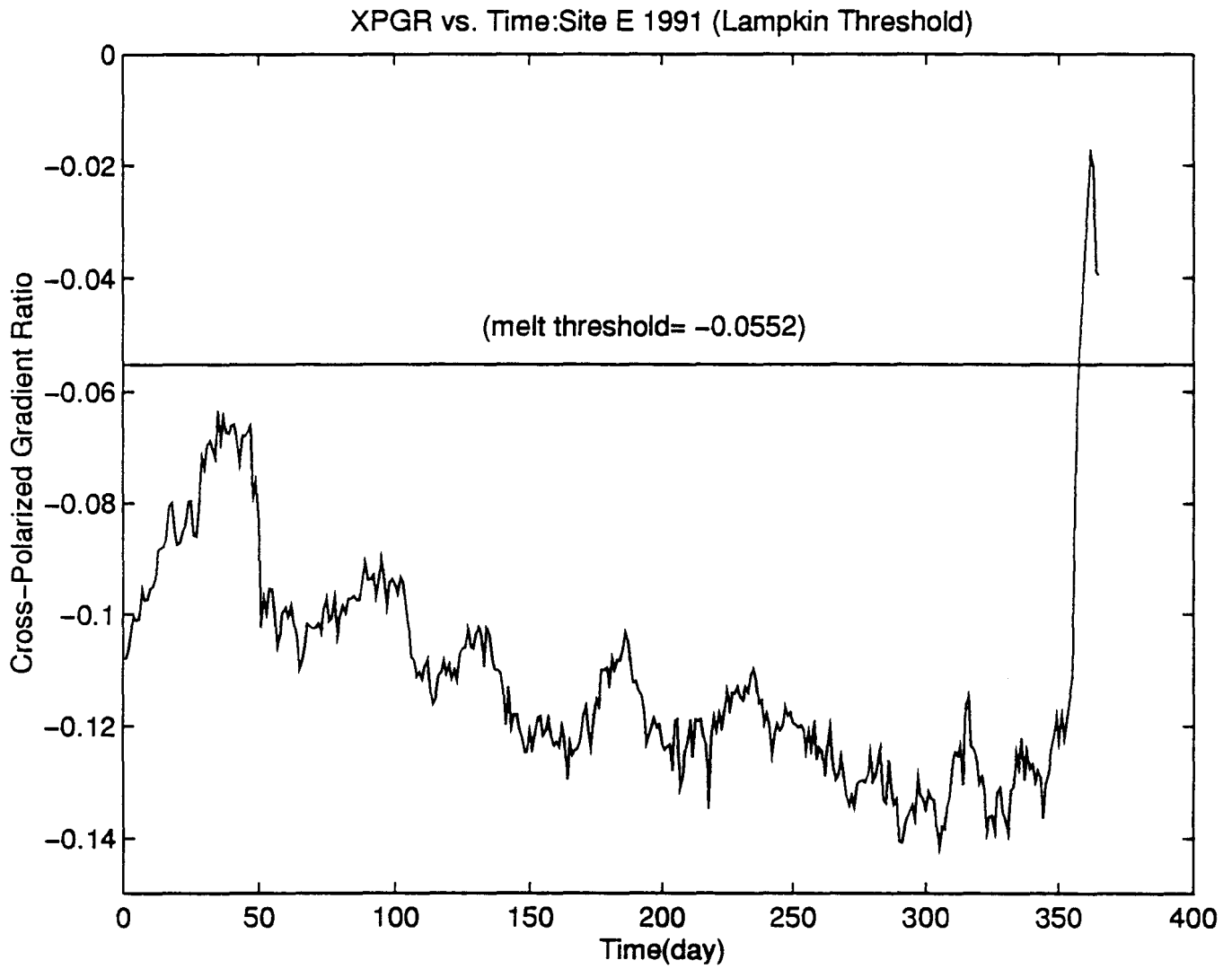


Figure 32. Graph of XPGR vs. time at Site E for the year of 1991.

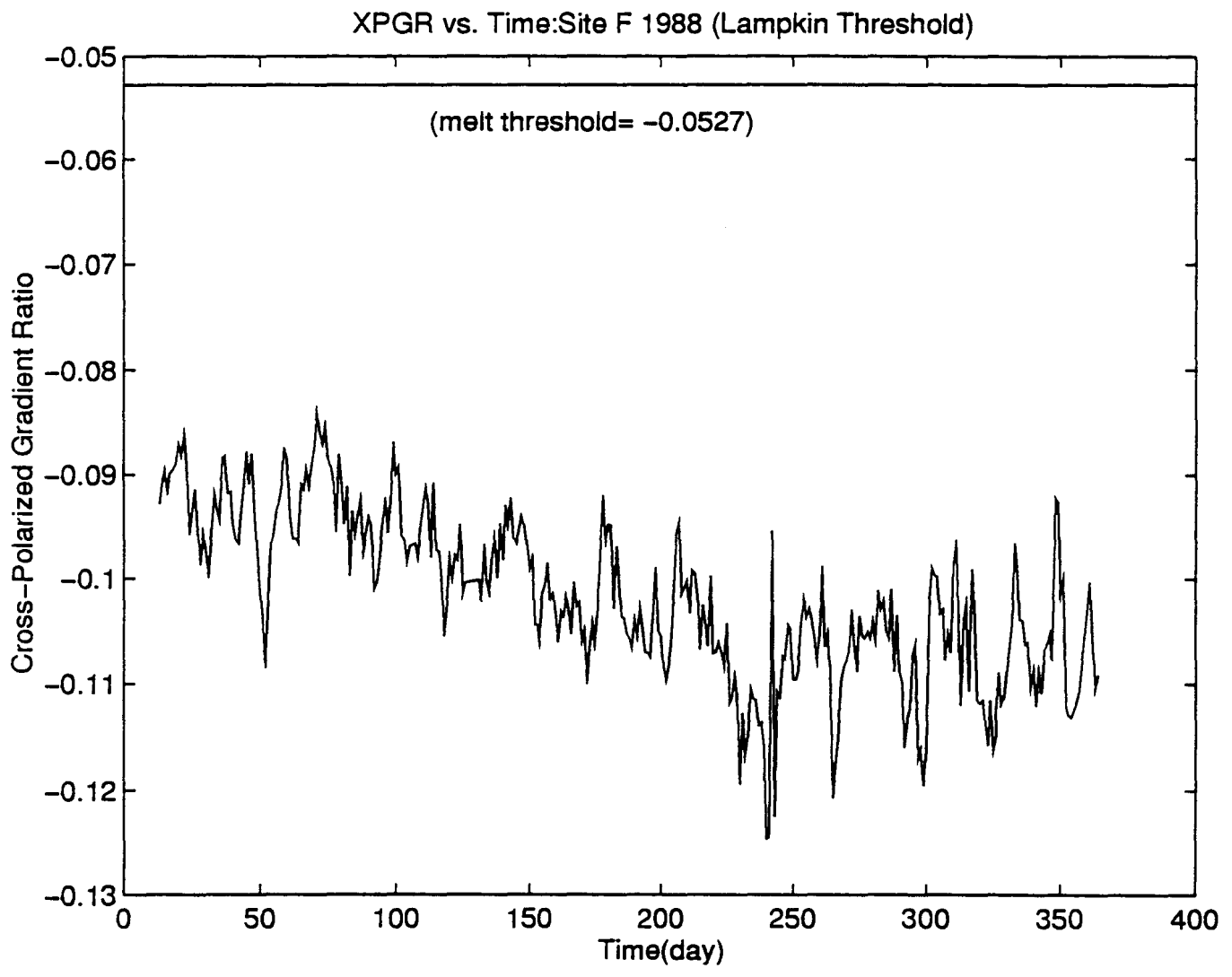


Figure 33. Graph of XPGR vs. time at Site F for the year of 1988.

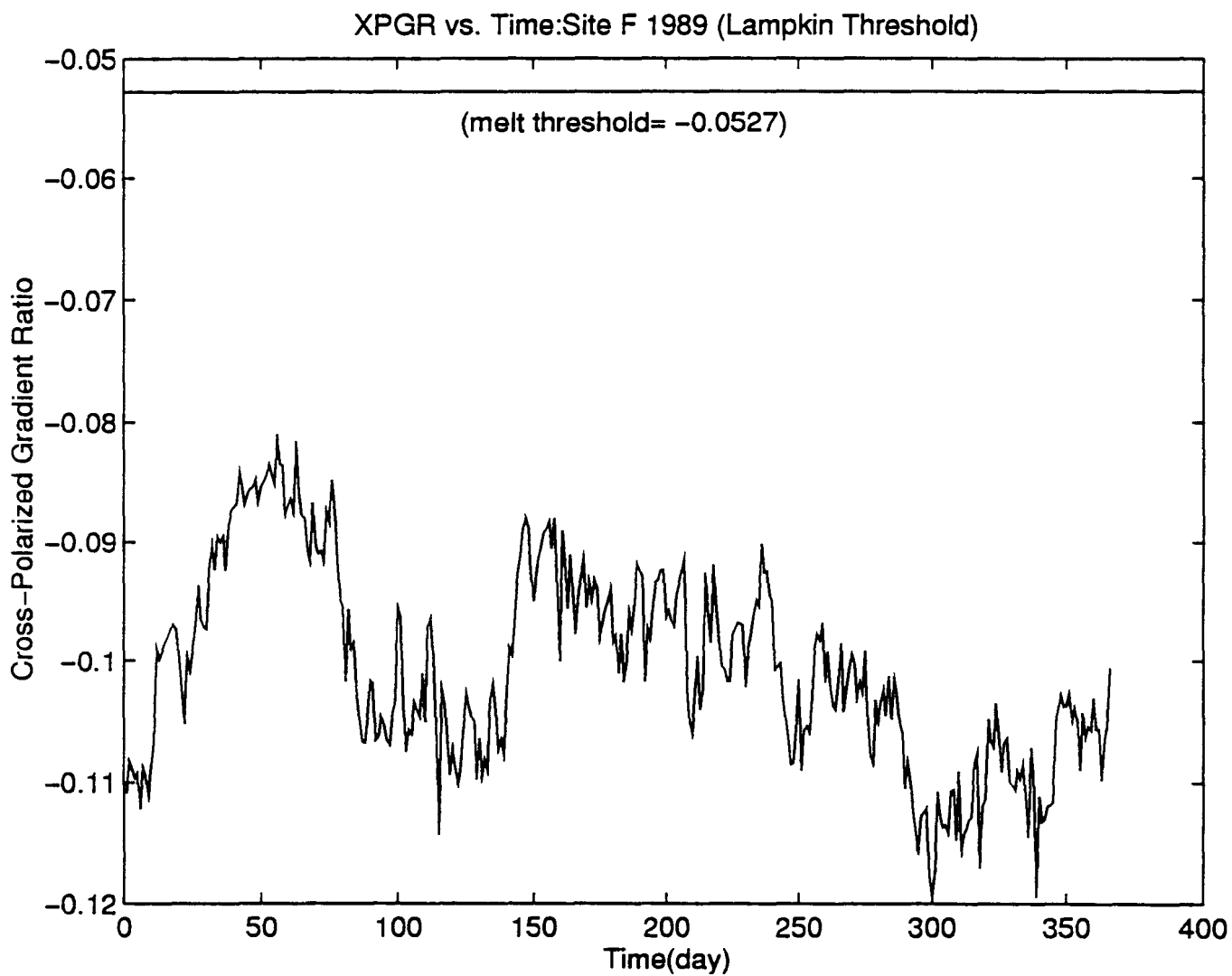


Figure 34. Graph of XPGR vs. time at Site F for the year of 1989.

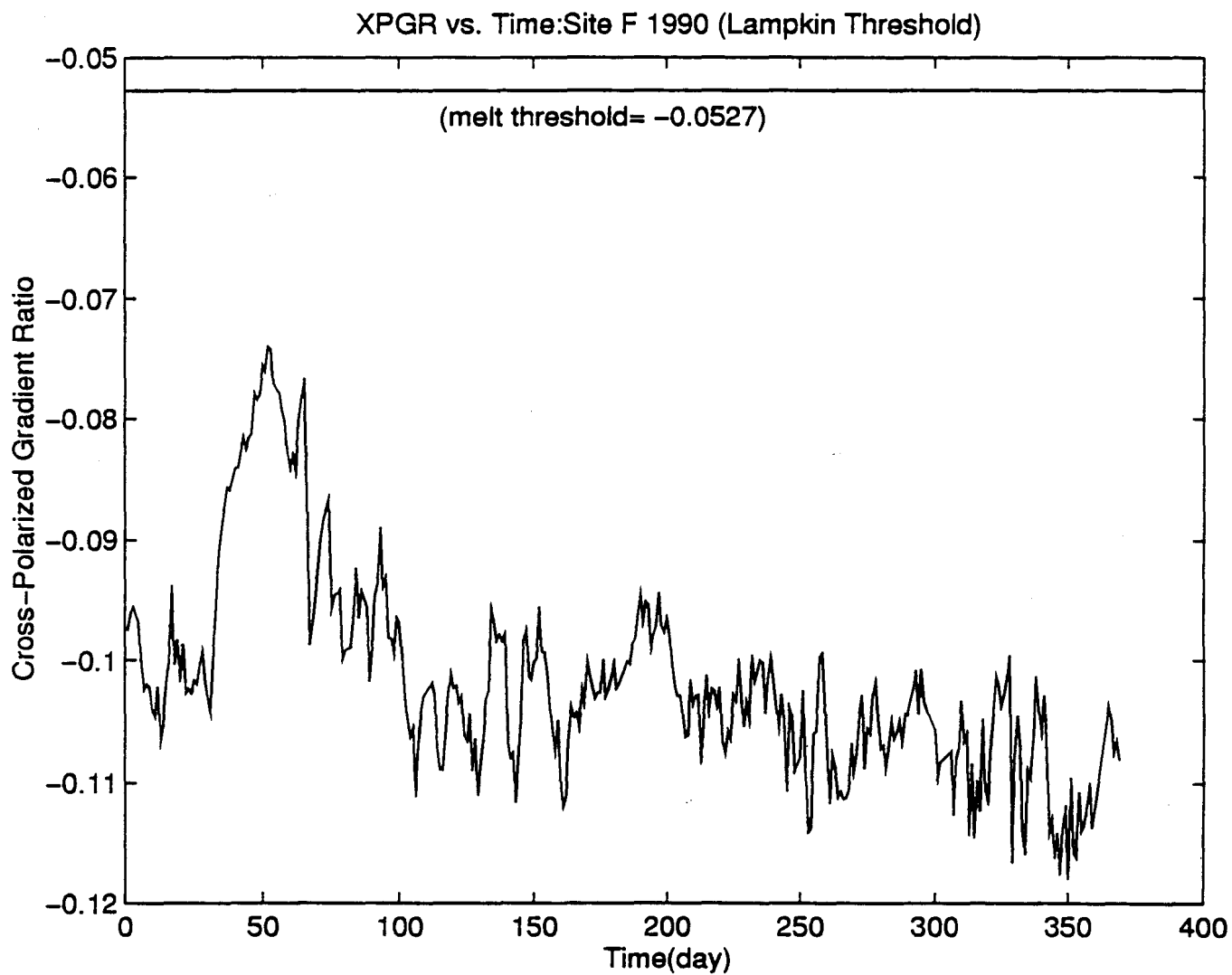


Figure 35. Graph of XPGR vs. time at Site F for the year of 1990.

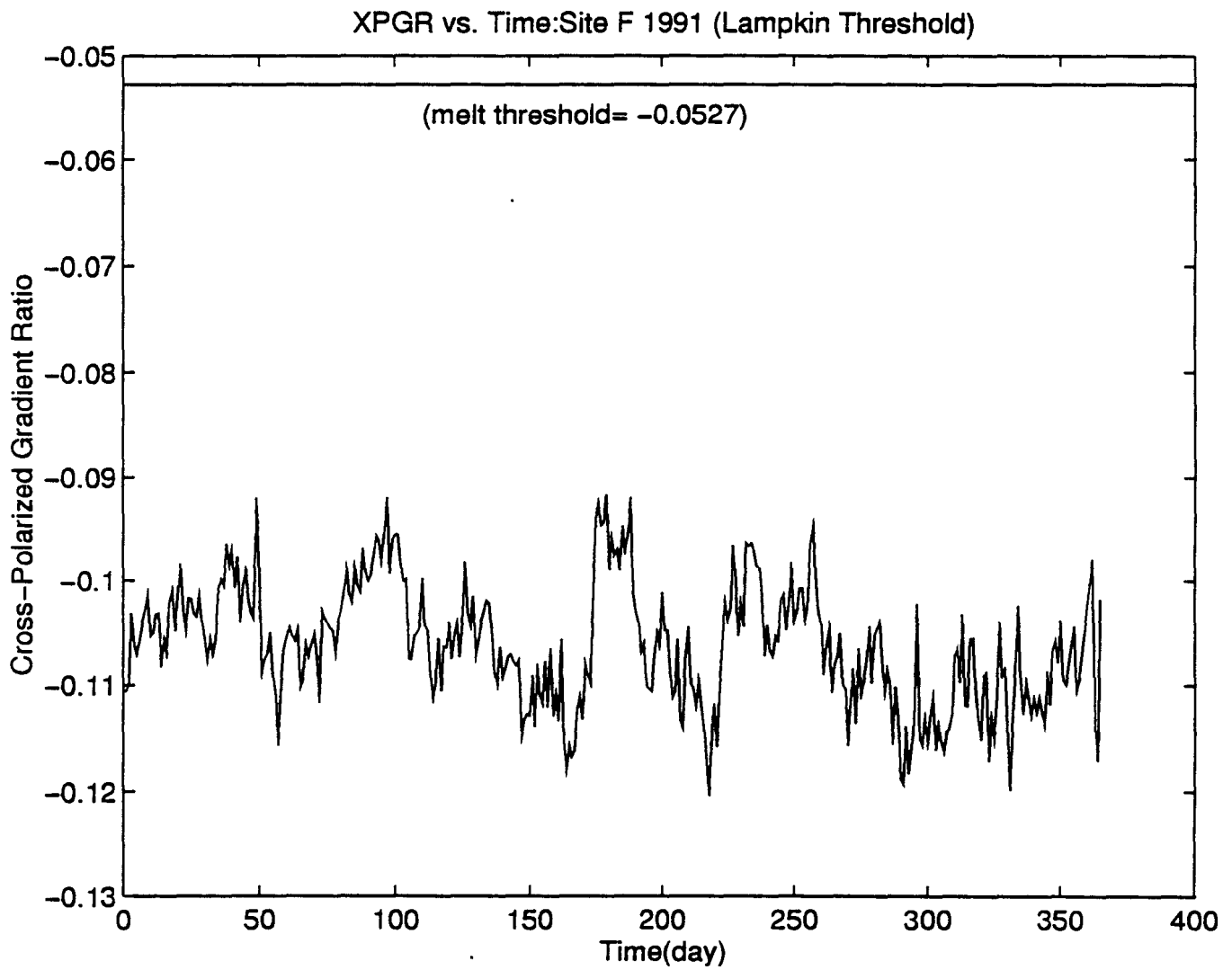


Figure 36. Graph of XPGR vs. time at Site F for the year of 1991.

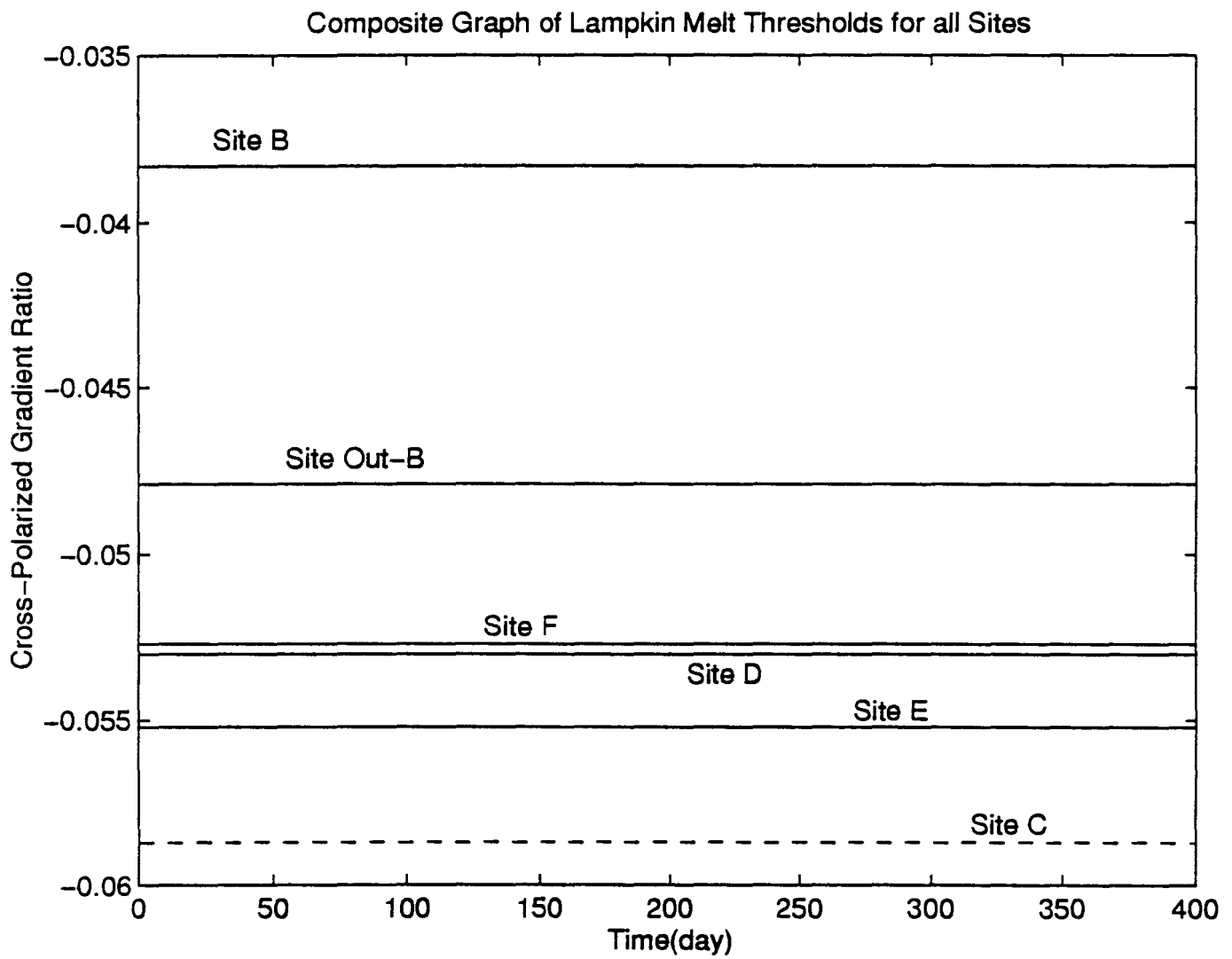


Figure 37. Composite graph of calculated melt thresholds for all sites.

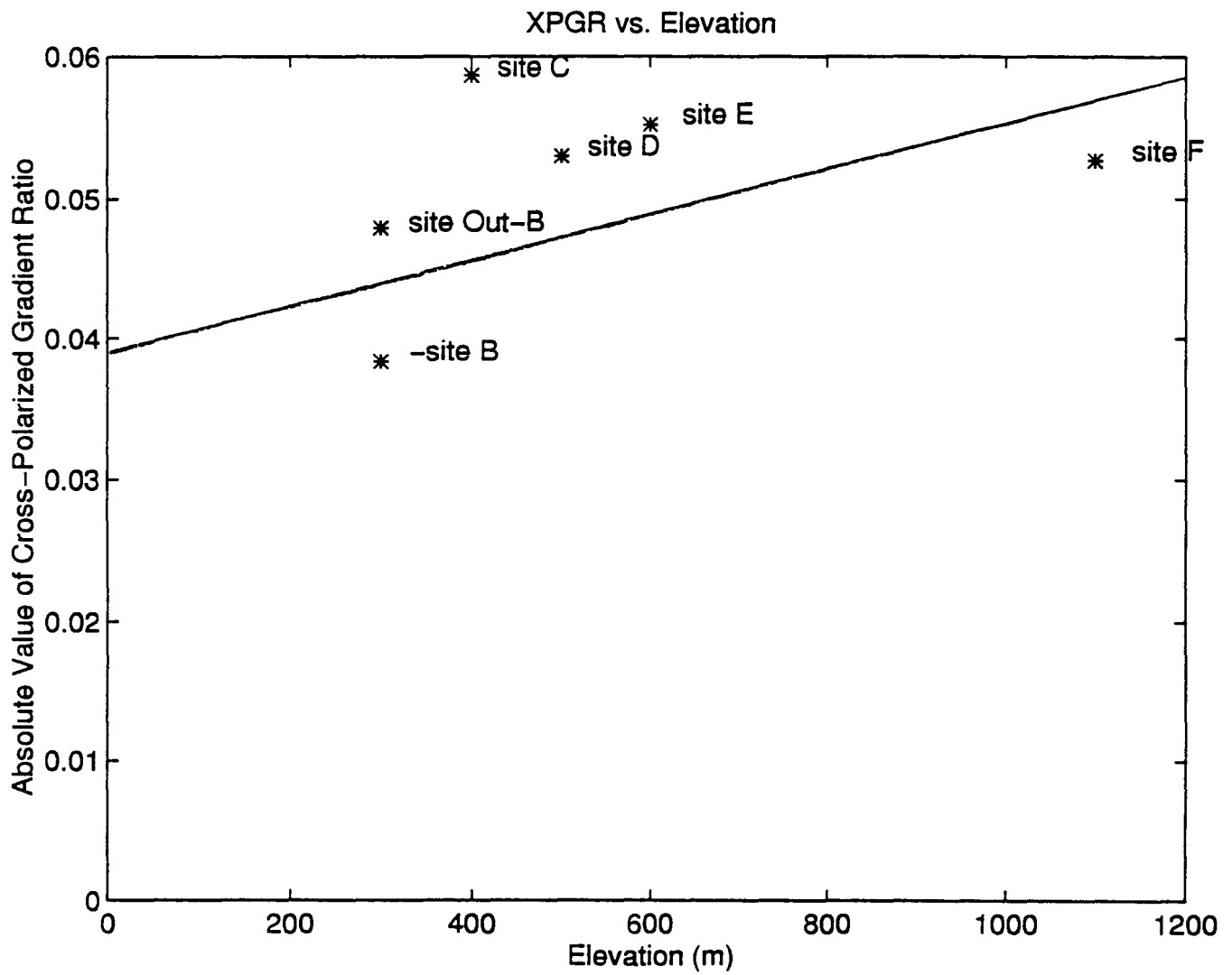


Figure 38. Graph of XPGR vs. Elevation. Notice weak linear relationship.

elevation may be weakly linear. This weak linear relationship may be dependant on several variables. One such variable that governs the behavior of Site C in the plots is the fact that its location is positioned in crevassed territory. Such a location may cause the XPGR to be lower due to large crevasses and air spaces occupying the ice streams. The decrease in XPGR under these conditions could be due to more volume scattering in the passive microwave signal.

Table III: Cross-Polarized Gradient Ratio Melt Threshold Values

Site	XPGR Melt Threshold	Elevation (m)
B	-0.0383	300
Out-B	-0.0479	300
D	-0.0530	500
F	-0.0527	1100
C	-0.0587	400
E	-0.0552	600

7.0 Ours vs. Theirs.

It is important to compare our melt scheme against the melt determining schemes of other researchers. To address this issue, various melt schemes by Abdalati and Steffen, (1995), Mote et. al, (1983), and Zwally and Fieglass, (1994) will be reviewed and compared to ours. Table IV. summarizes the melt schemes implemented by the listed researchers.

Table IV: Melt Determining Schemes by Various Researchers

Researchers	Methods
Abdalati and Steffen (1995)	- implements the XPGR algorithm on passive microwave data of Greenland and designates values less than -0.025 as melt values based on in situ observations.
Mote et. al (1993)	- calculates a mean winter brightness temperature value as melt threshold with a chosen offset value added. This is done for the 19GHz. vertical channel. This melt threshold is determined by in situ observation at Crawford Point in Greenland.
Zwally and Fiegler (1994)	- calculates a mean annual brightness temperature value with a 30K offset for the 19GHz horizontal channel.

Abdalati and Steffen method:

This research group implemented the XPGR algorithm and applied it to SSM/I passive microwave data spanning the period from January 1, 1988 through December 31, 1991 of Greenland. The passive microwave time-series data were compared to in situ measurements taken at the

Swiss Federal Institute of Technology (ETH) research camp at 69 34N, 49 17 W, 1155m. The time periods corresponding to prominent spikes in the XPGR show a mean water content in the polar firn at the research site of 0.5%. These time periods were identified as periods of melt at the research site, therefore Abdalati and Steffen (1995) fixed their melt threshold at XPGR= -0.025 (Abdalati and Steffen,1995). Abdalati and Steffen, (1995) compared their XPGR results to Mote et. al (1993) and Zwally and Fiegles (1994). They found that the difference between summer and winter 19v brightness temperatures is lower in colder regions than in warmer ones. From this, they conclude that melt events are not as likely to be detected when using a brightness temperature threshold alone.

Zwally and Fiegles Method:

Zwally and Fiegles conclude that three conditions could be useful in detecting melt events observed in the passive microwave data. These conditions in summary are: 1) an increase in Tb over an established threshold; 2) increase of Tb by an established amount over the calculated local mean summer value for periods where melting has not occurred; 3) an increase in Tb by a fixed amount over the local annual mean Tb (Zwally et. al, 1994). From these conditions, Zwally and Fiegles state that detection

of melt based on the last two conditions allows for more sensitivity to melt events. The emissivities of wet firn are essentially the same for vertical and horizontal polarizations. For dry firn, brightness temperatures for the horizontal polarization channel are generally lower. Hence Zwally & Fiegler, (1994) utilized the horizontal polarizations in their study because they would be more sensitive to large increases in the T_b as opposed to the vertical channels. Zwally & Fiegler, (1994) analysis of annual mean brightness temperature values compared to the mean summer brightness temperature values for the six regions in Antarctica. This prompted them to fix their melt threshold value as a fixed amount above the mean annual T_b . This value was fixed at 30K. This melt threshold value defined as $\langle T_b \rangle + 30$ was cited as being sufficiently large enough to overcome the effects of random noise in the passive microwave signal.

Note et. al Method:

Note et. al utilized the 19Ghz vertical channel in order to fix their melt threshold. They analyzed passive microwave time-series data from December 1, 1988 through February 1989 and from June 1, 1989 through July 31, 1989 for the following locations on the Greenland Ice Sheet: the ETH camp; NASA's New Crawford Point research camp; and the European

GRIP deep ice core drilling camp. Mote et. al used the difference between the mean summer and winter brightness temperatures for the 19GHz, vertical channel in order to fix their melt threshold. This research group states that this scheme was chosen to account for the variation in brightness temperatures prior to summer melt (Mote et. al, 1993). A 31K value above the winter mean was established by Mote et. al as their melt threshold value.

Lampkin Method:

Our melt threshold scheme, in comparison to the above, is very similar to that of Abdalati and Steffen, (1995) because we both utilized the XPGR algorithm. The difference lies in the application of the algorithm. Abdalati and Steffen, (1995) establish their melt threshold based on mean water concentration at a particular field site in Greenland. Our melt threshold was determined by a computed base XPGR value calculated from mean annual summer Tb values. Essentially we adopt parts of all three approaches.

Abdalati and Steffen compare their methods and results to that of Zwally and Fieglas, and Mote et. al. Abdalati and Steffen state that the differencing method utilized by Mote et. al identifies more melt events in the known cooler, northern regions than in the warmer southern regions.

They state that this may be due to the fact that the winter Tb values were higher in the warmer study area than in the cooler study area. They also state that in the warmer study area, the fewest melt events were identified with the differencing technique in a year that experienced the warmest mean winter brightness temperatures. Conversely, the melt threshold determined by Zwally Fieglass essentially is ad hoc. This value is based on Zwally Fieglass observations at six locations which cover large areas throughout the continent. These values are not applicable to smaller local regions where such a melt scheme may not be appropriate.

Our method uses a melt threshold value that is computed based on local summer means. While Abdalati and Steffen's use of in situ data yields a more physically-based threshold, absence of necessary wetness data precluded this approach in our case. We argue that our approach is superior to the one presented by Mote et. al for the reasons summarized in the above discussion. We also believe our approach is superior Zwally and Fieglass because it attempts to account for atmospheric effects.

8.0 Comparison with In Situ Data

The Lampkin Threshold technique predicts melt events at certain times in the year at various sites. These predictions should be manifest as ice lenses in the snow stratigraphy. Figure 4 is a sketch of the snow

stratigraphy at the Outer-B research camp. It was excavated during the 1993-94 Antarctic field season. The most prominent feature in the sketch is the thick ice lens positioned at a depth of about 1.22 meters. This ice lens is approximately 1.5 to 2 mm thick. It is reasonable to associate this particular ice lens with the 1988 melt event observed in the passive microwave data.

8.1 Accumulation Rate.

Passive microwave data and the XPGR melt algorithm to identify melt are useful tools for determining the accumulation rate of the areas identified as having experienced surface melting. The ice lens developed by the 1988 melt event and detected in the passive microwave data can be used as a time marker to determine the accumulation rate of regions where surface melting has occurred. The ice lens present in figure 4 is at approximately 1.22 meters depth. The surface of the snow column in the snow stratigraphy sketch corresponds to December of 1993 whereas the ice lens at depth corresponds to the December 1988 melt event. These horizons record a 5 year time span in accumulation. In calculating the accumulation rate of the Out-B region the mass of the snow column is determined by:

mass/per unit area of column= $\bar{\rho}$ X h

where:

$\bar{\rho}$ = average density of the snow column between the surface and the ice lens.

h= height of the snow column between the surface and the ice lens.

The density of the ice column is taken as approximately .38 grams/cc (personal communication with Ian Whilans, 1995). and the height of the column is approximately 122 cm. The mass of the column is 46.3 grams. The density of water is 1gram/cc. Since:

Density=mass/volume

the volume of the snow column is equal to:

$$(46.3 \text{ grams})/(1\text{gram/cc})=46.3 \text{ cc}$$

Since the time interval covering the construction of the snow column is 5 years the accumulation rate is determined by:

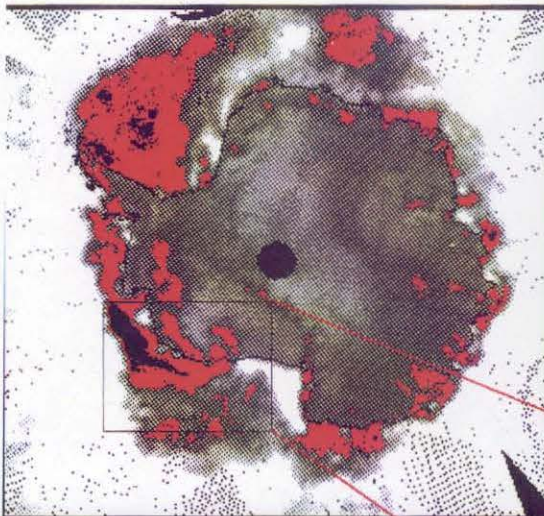
(46.3 cc) / 5 years

This calculation places the accumulation rate at 9.3 cm/ year per unit area. According to the value Alley, (1988) sites for the accumulation rate at Upstream B is 8.6 cm/year. Our value is within .7 cm/ year of previously derived values for the accumulation rate of this region.

9.0 Conclusion

This research project began with the observation of a high brightness temperature anomaly observed in 1988 over West Antarctica. The Tb anomaly was identified as a warm air storm phenomena in transit across Marie Byrd Land, West Antarctica over several days in December of 1988. The high Tb signature was attributed to surface melting. In order to map melt extent, several techniques for establishing a melt threshold were explored. A modified XPGR algorithm was found to be the most effective approach. Melt threshold values were calculated for various sites in Marie Byrd Land using a modified XPGR known as the Lampkin Technique. From this analysis, it was determined that the XPGR algorithm was site specific. The Lampkin Threshold was used to identify the 1988 melt event in in situ snow stratigraphic data from Out-B research camp. The ice horizon associated with this melt event was used as a time

marker to calculate the accumulation rate of the melt region. An averaged melt threshold value calculated from the melt thresholds of the 6 sites analyzed in this project was used to construct a passive microwave map outlining melt regions (see figure 39). Figure 39 is a melt map of December 15 1988, identifying melt regions (in red) according to our derived melt threshold. The inset shows the melt feature which corresponds to the high Tb anomaly. The Lampkin Technique will enable geophysicists and glaciologists to monitor significant melt events more efficiently, and determine regional accumulation rates of these melt regions.



December 15 1988

Figure 39.
Passive microwave map
highlighting melt regions (in red)
as determined by the Lampkin Melt Threshold.



Brightness Temperature anomaly
observed in the animated passive microwave
movie

References

- Abdalati, W. and K. Steffen,1995. Passive microwave-derived snow melt regions on the Greenland Ice Sheet. *Geophysical Research Letters*, Vol.22, No.7 (787-790).
- Alley, R.B,1988. Concerning the deposition and diagenesis of strata in Polar firn. *J. Glaciology*, Vol.34, No.118 (283-290).
- Bindshadler, R.A., K.C. Jezek, and J. Crawford,1987. Glaciological investigations using the synthetic aperture radar imaging system. *Annals of Glaciology*, *Annals of Glaciology*, Vol.9, (11-19).
- Gow, A. J,1968. Deep core studies of the accumulation and densification of snow at Byrd Station and Little America V, Antarctica. CRREL, Res. Rep., 197.
- Hollinger, J., R. Lo, G. Poe, R. Savage, and J. Peirce,1987. Special sensor microwave/ imager user's guide. Washington, D.C., Naval Research Laboratory.
- Keller, L.M., G.A. Weider, C.R. Stearns, and M.F. Sievers,1989. Antarctic automatic weather station data for the calendar year 1988. Department of Meteorology, University of Wisconsin.
- *Manual of Remote Sensing, Second Edition, Vol.1*, Robert N. Colwell, American Society of Photogrammetry, 1983.
- Matzler, C.H., and R. Hueppi,1989. Review of signature studies for microwave remote sensing of snowpacks. *Adv. Space Research*, 9(1), (253-265)

- Mote, T.L., M.R. Anderson, K.C. Kuivinen, and C.M. Rowe,1993. Passive microwave-derived spatial and temporal variations of summer melt on the Greenland ice sheet. *Annals of Glaciology*, No.17 (233-238).
- Schanda, E., 1986. *Physical fundamentals of remote sensing*, Springer-Verlag, Berlin; New York.
- Shuman, C.A., R.B. Alley, S. Anadkrishnan, and C.R. Stearns,1994. An empirical technique for estimating near-surface air temperature trends in Central Greenland from SSM/I brightness temperatures.
- Ulaby, F.T., R.K. Moore, and A.K. Fung,1982. *Microwave remote sensing, Vol. II: radar remote sensing and surface scattering and emission theory*. Artech House, Inc.
- Walker,A.E., and B.E. Goodison,1993. Discrimination of a wet snow cover using passive microwave satellite data. *Annals of Glaciology*, No.17 (307-311).
- Wilson, J.D., and K.C. Jezek,1993. Co-registration of an Antarctic digital elevation model with SSM/I brightness temperatures. *Annals of Glaciology*, No.17 (93-97).
- Zwally, H.J.,1977. Microwave emissivity and accumulation rate of polar firn. *Journal of Glaciology*, Vol.18, No79 (195-215).
- Zwally, H.J., and Per Gloersen,1977. Passive microwave images of the polar regions and research applications. *Polar Record*, No.18 (431-450).
- Zwally, H.J., R.A. Bindshadler, A.C. Brenner, T.V. Martin, and R.H. Thomas,1983. Surface elevation contours of Greenland and Antarctica ice sheets. *Journal of Glaciology*, Vol.88, No.C3 (1589-1596).

- Zwally, H.J., and S. Fieglas,1994. Extent and duration of Antarctic surface melting. Journal of Glaciology, Vol.40, No.136 (463-476).

Appendices

- Extract.C Program
- Locate.for Program

```

/*****
/* This program extracts a portion of an SSMI data file on CDROM, */
/* averages the values, and outputs them to a file. Input to this */
/* program is an x,y data file (points.dat) which was created by the */
/* program locate.c. The x,y data points represent those values in */
/* a SSMI file to be averaged. The output of this program is a file */
/* (results.dat) of the averaged values. If the file (results.dat) */
/* already exists the new data will be appended to the bottom of the */
/* file. This allows more than one CD of data to be examined. The */
/* user is prompted for the starting and ending month and year for */
/* the given CD and the program processes all files within this range */
/* The program is written to run on the SUN workstation but with */
/* slight modification it can run on any platform. The change is in */
/* function get_filename(). Change the first strcpy command to */
/* reflect the new path for a different machine. */
/* EX. change strcpy(infile, "/cdrom/s3b/19"); */
/* to strcpy(infile, "l:/s3b/19"); */
/* */
/* One additional change is to remove all calls to byte_swap() since */
/* byte swapping is not needed on the PCs */
/*****/

```

```

#include <stdio.h>
#include <stdlib.h>
#include <string.h>

```

```

FILE *data, *points, *outfile;
int x[104912], y[104912], index, start, finish;
char month[37], *date, smon[5], emon[5];

```

```

/*****/
/* initialize() opens the input and output data files and sets up the */
/* month array. */
/*****/
void initialize()

```

```

{
    if ((points=fopen("points.dat", "r")) == NULL)
    {
        printf("\nError points file not generated\n");
        exit(1);
    }

    if ((outfile=fopen("results.dat", "r")) == NULL)
    {
        if ((outfile=fopen("results.dat", "w")) == NULL)
        {
            printf("\nError could not open output file \n");
            exit(1);
        }
        fprintf(outfile, "\n DATE          19V          19H          22V          37V
7H\n\n");
    }
    else
    {

```

```

fclose(outfile);
if ((outfile=fopen("results.dat","a")) == NULL)
{
    printf("\nError opening file to append\n");
    exit(1);
}
}
strcpy(&month[0], "jan");
strcat(&month[3], "feb");
strcat(&month[6], "mar");
strcat(&month[9], "apr");
strcat(&month[12], "may");
strcat(&month[15], "jun");
strcat(&month[18], "jul");
strcat(&month[21], "aug");
strcat(&month[24], "sep");
strcat(&month[27], "oct");
strcat(&month[30], "nov");
strcat(&month[33], "dec");
date=(char *)malloc(7);
printf("\nStarting year and month (yyymm): ");
scanf("%s", smon);
start = atoi(smon);
printf("\nEnding year and month (yyymm): ");
scanf("%s", emon);
finish = atoi(emon);
}

/*****
/*  get_filename() determines which file is to be processed next      */
*****/

void get_filename(infile)
char *infile;
{
    char temp[3];
    int i;
    strcpy(infile, "/cdrom/s3b/19");
    strncat(infile, smon, 2);
    strcat(infile, "/");
    strncpy(temp, &smon[2], 2);
    i=(atoi(temp)-1)*3;
    strncat(infile, &month[i], 3);
    strcat(infile, "/");
    strcat(infile, smon);
    strcat(infile, "01");
    strcat(infile, ".s3b");
}

/*****
/*  byte_swap swaps the bytes of the 16 bit integer read in for      */
/*          processing on the SUN.                                     */
*****/
void byte_swap(number)
short int *number;

```

```

{
    unsigned short int left,right;

    left = right = *number;
    left = left << 8;
    right = right >> 8;
    *number = ((left | right));
}

/*****/
/* get_pts() reads in the set of x,y coordinates to use for      */
/*      averaging.                                              */
/*****/
void get_pts()
{
    index=1;
    fscanf(points,"%d %d\n",&y[0],&x[0]);
    while (!feof(points))
    {
        fscanf(points,"%d %d\n",&y[index],&x[index]);
        index++;
    }
}

/*****/
/* process() reads and averages all points requested for a given file */
/*      If a given value in the file is 0 the program does not      */
/*      include it in the averaging. This function also writes     */
/*      the data to the output file.                               */
/*****/
void process()
{
    int skip,i,j,total[5];
    short int *values;
    float *avalues;

    values = (short int *)malloc(5*2);
    avalues = (float *)malloc(5*sizeof(float));
    skip = ((y[0])*316)*10+x[0]*10;
    fseek(data, skip, 0);

/* Initialize variables */
    for(i=0;i<5;i++)
    {
        total[i]=0;
        avalues[i]=0;
    }

/* process all points for this file */
    for (i=1; i<index; i++)
    {
        fread(values,2,5,data);
        for(j=0; j<5; j++)
        {
            byte_swap(&values[j]);

```

```

        avalues[j]=avalues[j]+values[j];
        if (values[j] != 0)
            total[j] = total[j]+1;
    }

/* determine how many bytes to skip to the next requested value */
    skip = ((y[i]-y[i-1])*316-x[i-1])*10+(x[i]-1)*10;
    fseek(data, skip, 1);
}
fread(values,2,5,data);
for(j=0; j<5; j++)
{
    byte_swap(&values[j]);
    avalues[j]=avalues[j]+values[j];
    if (values[j] != 0)
        total[j] = total[j]+1;
}
fprintf(outfile,"%s",date);
for (i=0;i<5;i++)
{
    if (total[i] == 0)
        avalues[i]=0;
    else
        avalues[i]=avalues[i]/(total[i]*10.0);
    fprintf(outfile,"          %4.2f",avalues[i]);
}
fprintf(outfile,"\n");
free(values);
free(avalues);
}

/*****
/* main() processes all data files on a given CD and makes all calls */
/*      to process the data for an individual file.          */
/*****/
main()
{
    char *infile,ch[3];
    int i,j,size;

    if ((infile = (char *)malloc(80))==NULL)
    {
        printf("\nError allocating memory for infile\n");
        exit(1);
    }
    initialize();
    get_filename(infile);
    get_pts();
    for (j=start; j<finish+1; j++)
    {
        gcvt((double)j,4,smon);
        get_filename(infile);
        for (i=0; i<31; i++)
        {
            if (i<9)
            {

```



```
    strcpy(ch, "00");
    gcvt((double)(i+1), 1, &ch[1]);
}
else
    gcvt((double)(i+1), 2, ch);
size = strlen(infile);
strcpy(&infile[size-6], ch);
strcat(infile, ".s3b");
strncpy(date, &infile[size-10], 6);
if ((data=fopen(infile, "rb")) != NULL)
{
    process();
    fclose(data);
}
}
}
exit(0);
}
```



```

      program locate
cccccccccccccccccccccccccccccccccccccccccccccccccccccccccccccccccccccccccccccccc
c
c LOCATE - This program transforms I,J coordinates of an SSM/I grid cell
c           to latitude and longitude coordinates. This program provides
c           the inverse functions as well. LOCATE interfaces to the revised
c           forms of the subroutines, MAPXY and MAPLL.
c
c User-defined Paramters:
c
c   gtype   : Integer supplied by the user to describe one of the three
c             grid cell dimensions (12.5 km, 25.0 km, or 50.0 km).
c
c   ihem    : Integer supplied by the user to describe one of the two
c             polar regions (1=North , 2=South)
c
c   itrans  : Integer supplied by the user to describe the type of
c             transformation LOCATE will perform (1=I,J-to-Lat,Lon;
c             2=Lat,Lon-to-I,J)
c
c   i,j     : Integers supplied by the user when itrans = 1. These
c             integers describe the position of a cell in an SSM/I grid.
c
c   lat,lon : Reals supplied by the user when itrans = 2. These
c             integers describe the latitude and longitude in an SSM/I
c             grid which LOCATE will transform to an I,J grid cell position.
c             Note: All latitudes and longitudes must be entered as
c             positive numbers!
c
c Internal:
c
c   x,y     : Distance in kilometers from the origin of the grid
c             (ie., pole).
c
c   alat,
c   alon    : Computed latitude and longitude returned from MAPXY.
c
c   SGN     : Sign of the latitude (positive = north latitude,
c             negative = south latitude)
c
c   delta   : Meridian offset for the SSM/I grids (0 degrees for
c             the South Polar grids; 45 degrees for the North Polar
c             grids.
c
c   kk      : Integer variable used for reorientation of the grid. The
c             grid is 'flipped' in the Y direction for transformations.
c
c   SLAT    : Standard latitude for the SSM/I grids is 70 degrees.
c
c   numy    : Number of lines in an SSM/I grid. This attribute varies
c             for each of the six grids.
c
c   cell    : Size of the SSM/I grid ( 12.5 km, 25.0 km, 50.0 km)
c
c   xydist  : Distance from the origin of the grid in the cartesian plane.

```

```
c          The x-y coordinates for the edge of the lower left pixel
c          is (3850.0, 5350.0) for the northern grids and
c          (3950.0, 3950.0) for the southern grids.
```

```
c RE      : Radius of the earth in kilometers.
```

```
c E       : Eccentricity of the Hughes ellipsoid
```

```
c E2      : Eccentricity squared
```

```
c PI      : Pi
```

```
Written by V.J.Troisi - January, 1990
```

```
CCCCCCCCCCCCCCCCCCCCCCCCCCCCCCCCCCCCCCCCCCCCCCCCCCCCCCCCCCCCCCCC
```

```
real SLAT,E,RE,PI
real alat,alon,x,y
integer ihem,GTYPE
real lat, lon
real SGN, delta
integer numy(2,3)
real cell(3), xydist(2,2)
data numy / 896, 664, 448, 332, 224, 166 /
data cell / 12.5 , 25.0 , 50.0 /
data xydist / 3850.0 , 5350.0 , 3950.0 , 3950 /
```

```
SLAT = 70.
RE = 6378.273
E2 = .006693883
PI = 3.141592654
E = sqrt(E2)
```

```
c
c Query for the SSM/I grid cell size.
```

```
c
c print *,'Enter the grid cell dimension:'
c print *,' 1. 12.5 Km'
c print *,' 2. 25.0 Km'
c print *,' 3. 50.0 Km'
c read *,gtype
```

```
c
c Query for polar region of interest.
```

```
c
c print *,'Enter the hemisphere of interest:'
c print *,' 1. North'
c print *,' 2. South'
c read *,ihem
```

```
c
c Define the sign and meridian offset (delta) for the SSM/I grids.
```

```
c
c if (ihem.eq.1) then
c   SGN = 1.0
c   delta = 45.
c else
c   SGN = -1.0
c   delta = 0.0
c endif
```

```

C
C Query for translation type.
C
    print *, 'Enter one of the following transform functions:'
    print *, ' 1. Convert I,J to Latitude, Longitude'
    print *, ' 2. Convert Latitude, Longitude to I,J'
    read *, itrans
C
C Start translation
C
    if (itrans.eq.1) then
C
C Obtain the I,J position of the grid cell to transform to Latitude
C and Longitude
C
        print *, 'Enter i, j:'
        read *, i, j
C
C Convert I,J pairs to x and y distances from origin. The grid will be
C 'flipped' in the 'Y' direction.
C
        x=((i-1)*cell(gtype))-(xydist(1,ihem)-cell(gtype)/2.)
        kk=numy(ihem,gtype)-(j-1)
        y=((kk-1)*cell(gtype))-(xydist(2,ihem)-cell(gtype)/2.)
C
C Transform x and y distances to latitude and longitude
C
        call mapxy (x,y,alat,alon,SLAT,SGN,E,RE)
C
C Transform radians to degrees.
C
        alon=alon*180./PI
        alat=alat*180./PI
        alon=alon-delta
C
C Convert longitude to positive degrees
C
        if (alon.le.0.0) alon=alon+360.
        if (alon.ge.360.0) alon=alon-360.
C
C Print the latitude and longitude for the center of the I,J cell.
C
        print *,alat,alon
    else
C
C Obtain the latitude and longitude pair and transform to cell where
C that pair is located.
C
        print *, 'Enter latitude and longitude (positive values):'
        read *,lat,lon
C
C Transform degrees to radians
C
        alat=abs(lat)*PI/180.
        alon=(lon+delta)*PI/180.
C

```

```

c Transform latitude and longitude to x and y distances from origin
c
      call map11 (x,y,alat,along,SLAT,SGN,E,RE)
c
c Convert x and y distances from origin to I,J pair (ii,jj)
c
      ii=nint((x+xydist(1,ihem)-cell(gtype)/2.)/cell(gtype))+1
      jj=nint((y+xydist(2,ihem)-cell(gtype)/2.)/cell(gtype))+1
c
c Flip grid orientation in the 'Y' direction
c
      kk=numy(ihem,gtype)-(jj-1)
c
c Print the I,J location of the cell.
c
      print *,ii,kk

      endif
end

```

SUBROUTINE MAPXY (X,Y,ALAT,ALONG,SLAT,SGN,E,RE)

```

C$*****
C$
C$
C$ DESCRIPTION:
C$
C$ This subroutine converts from Polar Stereographic (X,Y) coordinates
C$ to geodetic latitude and longitude for the polar regions. The equations
C$ are from Snyder, J. P., 1982, Map Projections Used by the U.S.
C$ Geological Survey, Geological Survey Bulletin 1532, U.S. Government
C$ Printing Office. See JPL Technical Memorandum 3349-85-101 for further
C$ details.
C$
C$
C$ ARGUMENTS:
C$
C$ Variable      Type      I/O      Description
C$
C$ X              REAL*4      I        Polar Stereographic X Coordinate (km)
C$ Y              REAL*4      I        Polar Stereographic Y Coordinate (km)
C$ ALAT           REAL*4      O        Geodetic Latitude (degrees, +90 to -90)
C$ ALONG          REAL*4      O        Geodetic Longitude (degrees, 0 to 360)
C$
C$
C$           Written by C. S. Morris - April 29, 1985
C$           Revised by C. S. Morris - December 11, 1985
C$
C$           Revised by V. J. Troisi - January 1990
C$           SGN - provide hemisphere dependency (+/- 1)
C$
C$*****
      REAL*4 X,Y,ALAT,ALONG,E,E2,CDR,PI
C$*****
C$

```

```
C$ DEFINITION OF CONSTANTS: *
C$ *
C$ Conversion constant from degrees to radians = 57.29577951. *
   CDR=57.29577951
   E2=E*E
C$ Pi=3.141592654. *
   PI=3.141592654
```

```
C$ *****
C$ SL = SLAT*PI/180.
200 RHO=SQRT(X**2+Y**2)
   IF (RHO.GT.0.1) GOTO 250
   ALAT=90.*SGN
   ALONG=0.0
   GOTO 999
250 CM=COS(SL)/SQRT(1.0-E2*(SIN(SL)**2))
   T=TAN((PI/4.0)-(SL/(2.0)))/((1.0-E*SIN(SL)))/
   C(1.0+E*SIN(SL))**(E/2.0)
   IF (ABS(SLAT-90.) .LT. 1.E-5) THEN
   T=RHO*SQRT((1.+E)**(1.+E)*(1.-E)**(1.-E))/2./RE
   ELSE
   T=RHO*T/(RE*CM)
   END IF
   CHI=(PI/2.0)-2.0*ATAN(T)
   ALAT=CHI+((E2/2.0)+(5.0*E2**2.0/24.0)+(E2**3.0/12.0))*SIN(2*CHI)+
   C((7.0*E2**2.0/48.0)+(29.0*E2**3/240.0))*SIN(4.0*CHI)+
   C(7.0*E2**3.0/120.0)*SIN(6.0*CHI)
   ALAT=SGN*ALAT
   ALONG=ATAN2(SGN*X,-SGN*Y)
   ALONG=SGN*ALONG
999 CONTINUE
   END
```

C
C

SUBROUTINE MAPLL (X,Y,ALAT,ALONG,SLAT,SGN,E,RE)

```
C$ *****
C$ *
C$ *
C$ DESCRIPTION: *
C$ *
C$ This subroutine converts from geodetic latitude and longitude to Polar *
C$ Stereographic (X,Y) coordinates for the polar regions. The equations *
C$ are from Snyder, J. P., 1982, Map Projections Used by the U.S. *
C$ Geological Survey, Geological Survey Bulletin 1532, U.S. Government *
C$ Printing Office. See JPL Technical Memorandum 3349-85-101 for further *
C$ details. *
C$ *
C$ ARGUMENTS: *
C$ *
C$ Variable Type I/O Description *
C$ *
```

```

C$  ALAT      REAL*4      I      Geodetic Latitude (degrees, +90 to -90) *
C$  ALONG     REAL*4      I      Geodetic Longitude (degrees, 0 to 360) *
C$  X         REAL*4      O      Polar Stereographic X Coordinate (km) *
C$  Y         REAL*4      O      Polar Stereographic Y Coordinate (km) *
C$
C$
C$          Written by C. S. Morris - April 29, 1985 *
C$          Revised by C. S. Morris - December 11, 1985 *
C$
C$          Revised by V. J. Troisi - January 1990 *
C$          SGN - provides hemisphere dependency (+/- 1) *
C$*****
C$          REAL*4 X, Y, ALAT, ALONG, E, E2, CDR, PI, SLAT, MC *****
C$*****
C$
C$  DEFINITION OF CONSTANTS: *
C$
C$  Conversion constant from degrees to radians = 57.29577951. *
C$  CDR=57.29577951
C$  E2=E*E
C$  Pi=3.141592654. *
C$  PI=3.141592654
C$
C$*****
C  Compute X and Y in grid coordinates.
  IF (ABS(ALAT).LT.PI/2.) GOTO 250
  X=0.0
  Y=0.0
  GOTO 999
250 CONTINUE
  T=TAN(PI/4.-ALAT/2.)/((1.-E*SIN(ALAT))/(1.+E*SIN(ALAT)))** (E/2.)
  IF (ABS(90.-SLAT).LT.1.E-5) THEN
  RHO=2.*RE*T/((1.+E)** (1.+E) * (1.-E)** (1.-E))** (E/2.)
  ELSE
  SL=SLAT*PI/180.
  TC=TAN(PI/4.-SL/2.)/((1.-E*SIN(SL))/(1.+E*SIN(SL)))** (E/2.)
  MC=COS(SL)/SQRT(1.0-E2*(SIN(SL)**2))
  RHO=RE*MC*T/TC
  END IF
  Y=-RHO*SGN*COS(SGN*ALONG)
  X= RHO*SGN*SIN(SGN*ALONG)
  print *, 'x=', X
  print *, 'y=', Y
999 CONTINUE
  END

```